Influence of the previous North Atlantic Oscillation (NAO) on the spring dust aerosols over North China

Yan Li[1], Falei Xu[1], Juan Feng[2], Mengying Du[1], Wenjun Song[1], Chao Li[1,3], and Wenjing Zhao[1,4]

[1]Key Laboratory for Semi-Arid Climate Change of the Ministry of Education, College of Atmospheric Sciences, Lanzhou University, Lanzhou, China

[2]State Key Laboratory of Remote Sensing Science, College of Global Change and Earth System Science, Beijing Normal University, Beijing, China

[3]Hubei Key Laboratory for Heavy Rain Monitoring and Warning Research, Institute of Heavy Rain, China Meteorological Administration, Wuhan, China

[4]Gansu Meterological Service Center, Lanzhou, China

Correspondence: Juan Feng (fengjuan@bnu.edu.cn)

Abstract. The North Atlantic Oscillation (NAO) has been confirmed to be closely related to the weather-climate in many regions of the Northern Hemisphere, however, its effect and mechanism upon the formation of ~~regional~~ dust events (DEs) have rarely been involved in China. By using the station observation data~~set~~, and multi reanalysis datasets, ~~the influence of NAO on the dust aerosols (DAs) in China, as well as the corresponding mechanism of synoptic cause are explored in perspective of transient eddy fluxes. I~~it is found that the spring dust aerosols (DAs)~~DAs~~ in North China (30 °-40 °N, 105 °-120 °E) , a non-dust source region,~~in the non-dust source areas~~ show high values with a strong inter-annual variability ~~in north of the Yangtze River (30 °-40 °N, 105 °-120 °E), which is referred to as the North China hereafter.~~ and the spring DAs in North China is significantly correlated with the previous winter NAO~~A significant negative relationship is indicated between the boreal winter NAO index and the late spring DAs in the North China with the correlation coefficient of -0.39.~~ According to the 9 spring DEs affected significantly by negative phase of the preceding winter NAO in the North China during 1980-2020, it is shown that before the outbreak of DEs, due

to the transient eddy momentum (heat) convergence (divergence) over the dust aerosol (DA) source

regions, the zonal wind speed increases in upper-level troposphere, strengthening the zonal wind in

the middle-lower levels through momentum downward transmission. Simultaneously, there is

transient eddy momentum (heat) divergence (convergence) around the Ural Mountains, which is

favorable for establishment and maintenance of the Ural ~~ridge~~Ridge, as well as development of the

air temperature and vorticity advections. The combined action of temperature and vorticity

advections results in the Siberian Highs and Mongolian cyclone to establish, strengthen, and move

southward near the surface, guiding the cold air from high latitudes southward, and is favorable to

the uplift and transmission of DAs to the downstream North China. Simultaneously, the changes in

upstream transient eddy flux transport cause both energy and mass divergence in North China,

resulting in diminishing winds during DEs, which will facilitate the maintenance of dust aerosols

here and promote the outbreak of DEs. ~~After the outbreak of DEs, change of transient eddy fluxes~~

~~in the DA source regions and the Urals regions, leads to both energy and mass divergence and~~

~~reduction of the zonal winds over the North China. Accompanying with the prevailing southerly~~

~~airflow in south of the North China, a stable high value of DA concentration is maintained for 1-2~~

~~days.~~ This study reveals the impact of transient eddy fluxes transport on the dusty weather anomalies

modulated by the NAO negative signal in the North China, which can deepen the understanding of

formation mechanism of DEs in China.

1 Introduction

Airborne dust aerosols (DAs), which play a significant role in the evolution of the atmospheric

system, have an important influence on human society, ecosystems, and biochemical cycles. In

particular, the radiative forcing of DAs is comparable to that of clouds on a regional-scale and has

a key impact on the local weather-climate (Kaufman et al., 2002; Huang et al., 2014a; Yang et al.,

2017). Recently, the influence of DAs on the weather-climate has attracted widespread attention

from researchers, and the direct, indirect and semi-direct feedback responses between them have

been confirmed by scientific studies. For direct processes, DAs can impact the weather-climate by

scattering (absorbing) ~~shortwave and longwave~~ radiation to cool (heat) the atmosphere ~~or by~~

~~absorbing longwave radiation and solar shortwave radiation released by the earth and clouds to heat~~

~~the atmosphere~~ (Sokolik and Toon, 1996; Zhang et al., 2019); via indirect influence, DAs can change

58 ~~the local rainfall processes as well as~~ the albedo of ice and snow surfaces by altering the

59 characteristics of cloud condensation nuclei and ice nuclei (Ackerman et al., 2000; Sassen et al.,

60 2003); and in the semi-direct effects, DAs can increase cloud droplet evaporation and reduce cloud

61 water pathways by heating the clouds (Huang et al., 2006). ~~In addition, it has been found that due~~

62 ~~to the increase of DAs in the Arabian Sea, Arabian Peninsula, and West Asia, the Indian summer~~

63 ~~monsoon will be enhanced and thus influence the rainfall in central India (Jin et al., 2016).~~ The DAs

64 of worldwide annual emissions in the range of 1000-2150 Tg are lifted up by the surface wind

65 (Zender et al., 2004), with only approximately 30% of these resettles in the dust aerosol (DA) source

66 regions, while the other 70% is transported to downstream areas thousands of kilometres away,

67 causing changes in the local weather-climate (Duce et al., 1980; Huang et al., 2015).

68   One of the most serious natural catastrophes in East Asia is dusty weather. Studying the

69 climatological features, variations, and influencing factors of DAs are crucial to both understanding

70 and predicting DA variation patterns (Feng et al., 2020; Yao et al., 2021). Extensive analysis of

71 meteorological and climatic factors associated with the occurrence of global dust events (DEs) have

72 been conducted using ground-based observations (e.g., Ji and Fan, 2019; Liu et al., 2020), satellite

73 remote sensing (e.g., Chiapello et al., 2005; Han et al., 2022), and numerical simulations (e.g.,

74 Ginoux et al., 2004; Chen et al., 2017). It is concluded that the variations in DA concentration and

75 transport are related to many factors, including atmospheric circulation (Huang et al., 2021), surface

76 wind (Liu et al., 2004; Wang et al., 2018), cyclone frequency (Yu et al., 2019), Asian monsoon

77 (Wilcox et al., 2020), and the North Atlantic Oscillation (NAO) (Mao et al., 2011; Feng et al., 2019;

78 Li et al., 2019a;). The deserts in northern and western China and Mongolia are the most important

79 areas affecting China (primarily Badain Juran and Taklimakan), and the DAs in the above source

80 areas contribute 70% of the dust emissions in East Asia (Zhang et al., 2003; Che et al., 2019).

81 Therefore, it is of great significance to explore the characteristics and causes of DAs.

82   ~~According to statistical analysis, the annual dust emissions in northern China are approximately~~

83 ~~25 Tg, of which spring emissions account for over half (Xuan et al., 2000).~~ Recently, DEs seem to

84 be frequent in China, seriously endangering human health, hindering socioeconomic development

85 and causing widespread concern among the scientific community and the public. For example, from

86 14-16 March 2021, a large-scale dust event (DE) occurred in northern China (Yin et al., 2021),

resulting in more than 3.8 million km^2 affected, with the maximum hourly average concentration of

PM_{10} surpassing 8000 um_m^{-3} and a drop in visibility to less than 0.5 km in Beijing (Zhang et al.,

2022). ~~In addition, approximately 800 Tg of DAs in China are emitted into the atmosphere every~~

~~year, nearly half of the global emissions (Zhang et al., 1997).~~ In China, strong DEs can transport

DAs to Japan, Korea and even across the Pacific Ocean to the North American coast, reflecting the

fact that regional DEs in China can evolve into hemispheric and even global-scale phenomenon

(Kurosaki and Mikami, 2003; Lee and Sohn, 2009). According to previous studies, spring is the

most active time for the occurrence of DEs in China, accounting for over 80% of all DEs yearly

(Liu et al., 2004).Therefore, it is ~~of~~ important practical and scientific value and relevance to

investigate the formation mechanism of DEs in China, especially in spring.

In the Northern Hemisphere (NH), the NAO is a seesaw mode of centre pressure variation

(Walker, 1924) near the Azores and Iceland, and is the most important low-frequency dipole pattern

during boreal winter. The NAO has crucial effects on temperature (e.g., Hurrell, 1995; Yu et al.,

2016), precipitation (e.g., Hartley and Keables, 1998; Giannini et al., 2000), and storm tracks (e.g.,

Lau and Nath, 1991; Jin et al., 2006) in the North Atlantic and its surrounding areas. However, its

signal can also be used as a mediator waveguide through the midlatitude westerly wind belts,

capturing the downstream propagating Rossby wave train and thus extending its effect to the

weather-climate of the Eurasian continent, as well as the entire NH (e.g., Watanabe, 2004; Lin et al.,

2011; Zhang et al., 2021). China is located downstream of the NAO-connected circulation system,

and its weather (e.g., Wang and Shi, 2001; Liu et al., 2001; Zuo et al., 2015) and climate (e.g., Liu

et al., 2018; Li et al., 2021a; Yao et al., 2022) is impacted by variations in different phases and

intensities of the NAO. ~~For example, when the NAO is unusually strong in winter, China will be~~

~~controlled by an abnormally warm and rainy climate during the same period, and the temperature~~

~~in the Yangtze-Huaihe River Basin will be abnormally cooler in the next summer (Wang and Shi,~~

~~2001). Liu et al. (2001) found that changes in the NAO can alter the temporal and spatial~~

~~distributions of precipitation in the eastern Tibetan Plateau in summer by affecting the tropospheric~~

~~zonal winds. The NAO also has a key influence on weather-scale anomalies in China. Li et al.~~

~~(2021a) explored the connection between the NAO and persistent haze events in Beijing and found~~

~~that the NAO negative signal can modulate wave train transmission to northern China, exacerbating~~

~~the haze duration in Beijing. Yao et al. (2022) indicated that under the influence of seasonal accumulation of the NAO negative signal, the polar vortex will become more vulnerable and unstable compared to the climatic mean value, which will lead to more extreme cold occurrences in China.~~

Meanwhile, it has been shown that the NAO also has a crucial influence on the process of DEs in China. For example, Tang et al. (2005) noted that the frequency of spring DEs in northern China was significantly influenced by fluctuations in the NAO intensity. In addition, Zhao et al. (2012) discovered an obvious negative correlation between the winter NAO intensity and the late spring and summer DEs in northwestern China. The above studies mainly analysed the association between the NAO and the DEs in China from the perspective of seasonal-scale climate. However, the influence of weather-scale meteorological elements on DEs is also important (Wang et al.,2009; An et al., 2018). ~~For example, Qian et al. (2002) explored the connection between Chinese DEs and cyclonic activities from 1948 to 1999 and found a highly positive correlation between them. Wang et al. (2009) further discovered that the spring DEs in northern China were mostly near the centre of the Mongolian Cyclone (MC). Hara et al. (2006) used a regional-scale DA transport model and found that the frequency of DEs in the Gobi Desert of East Asia can also be increased by the intrusion of polar cold air. Furthermore, An et al. (2018) discovered that the decline in the strength and frequency of DEs in East Asia during the period of 2007-2016 was highly associated with the weakening tendency of strong winds following the entrance of higher-latitude cold air.~~ As mentioned previously, the large-scale climate variability model of the NAO can capture the Rossby wave train propagating downstream, which in turn has a crucial effect on the weather-scale elements. As one of the two fundamental fluctuations in the atmosphere, transient eddy is widely used in studies to diagnose Rossby wave trains (Trenberth, 1986) and can provide a perspective of mechanism exploration in abnormal variations in atmospheric circulation (Li et al., 2022). It has been noted that transient eddy has a sustained impact on the development of atmospheric systems such as the Siberian Highs (SH) as well as the North Pacific low (Holopainen and Oort, 1981; Holopainen et al., 1982). The forcing impact of transient eddy on the mean airflow can enhance anticyclonic circulation, which in turn may trigger large-scale severe low-temperature occurrences (Li et al., 2019b). In addition, Li et al. (2022) showed that transient eddy played a significant role

145 in the formation of abnormal atmospheric circulation of DEs by focusing on the spring DEs in south

146 Xinjiang, China, during 1980-2018.

147   It is essential to continue deep study of the synoptic mechanism of DE formation through the

148 aspect of the NAO. On the one hand, with the recent huge energy consumption and astounding

149 economic development in East Asia, the eastern part of China has suffered from escalating air

150 pollution problems (Zhang et al., 2012; Zhao et al., 2016). With the occurrence of DEs, DAs are one

151 of the most crucial elements affecting air quality in East Asia (Huang et al., 2014b; Nie et al., 2015).

152 Previous studies have provided some analysis and initial progress on the relationship between the

153 NAO and the DEs in northern China regions, mainly DA source areas such as northwestern China

154 (Tang et al., 2005; Zhao et al., 2012). However, such studies are limited to the eastern part of China,

155 which is not a DA source area but is severely affected by DEs. On the other hand, previous studies

156 of the NAO on the DEs in China have mainly been analysed on the seasonal-scale to provide a large-

157 scale climatic background for the occurrence of DEs in China, but it is not clear how the NAO

158 affects the DEs in China at the synoptic-scale, and the role of transient eddy in the anomalous

159 circulation of the atmosphere in DEs under the modulation of the NAO is uncertain.

160   From the above points of view, we investigated three main scientific questions in this paper: 1)

161 Does the NAO affect the area with high values of DAs in eastern China? What are the characteristics

162 of the impact? 2) What are the synoptic causes of the formation of DEs influenced by the NAO? 3)

163 How can we explain the mechanism of the formation of synoptic system anomalies by transient

164 eddy under NAO modulation? To address the above issues, by using station observation data, the

165 multi reanalysisMERRA-2 dataset, and reanalysis datasets from 1980-2020, this paper investigated

166 the long-term changes in the spring DAs in China to examine the characteristics of the impact of

167 NAO on the DAs in eastern China during the previous period and the same period, and to explore

168 the atmospheric circulation mechanisms affecting DEs considering transient eddy flux transport

169 under the influence of the NAO. The remaining work is organized as follows. Section 2 describes

170 the datasets and methods employed in this paper. Sections 3.1, 3.2, and 3.3 cover the selection of

171 DA study area and its link with the NAO, the process of abnormal atmospheric circulation during

172 DEs, and the impacts of the transport features of transient eddy fluxes accompanying synoptic

173 system anomalies, respectively. Section 4 contains the conclusions and discussions.

2 Datasets and methods

2.1 Datasets

The China National Meteorological Center (CNMC) provides the daily DE occurrence dataset over mainland China, which contains three types of DEs (dust storm, blowing dust, and floating dust). When DAs are transported with visibility less than 1 km, it is considered a dust storm, whereas floating dust with visibility less than 10 km is caused by DAs from upwind source regions, and blowing dust is defined similarly to floating dust, with the difference that the DAs are emitted from local source areas. Several previous studies have confirmed the validity of the dataset (Kang et al., 2016; Wang et al., 2018).

Datasets of daily and monthly DA concentrations under the Modern-Era Retrospective Analysis for Research and Applications, version 2 (MERRA-2), were derived from the Global Modeling and Assimilation Office (GMAO) of the National Aeronautics and Space Administration (NASA) (Gelaro et al., 2017). Its foundation is built on the assimilation of multiple satellite systems (AVHRR, MISR, MODIS) and AERONET ground-based observations, and the correctness and reliability are considered to be better than those obtained from the assimilation of individual satellites. ~~The MERRA-2 DA dataset is used for the Goddard Earth Observing System Model, version 5 (GEO-5) (Molod et al., 2015) and the grid statistical interpolation analysis method for three-dimensional variable assimilation (3DVar) (Kleist et al., 2009)~~. The most significant benefit of the MERRA-2 dataset is the spatiotemporal~~temporal and spatial~~ coherence, which cannot be surpassed by station-based or individual satellite data and allow for rigorous statistical analysis of the spatiotemporal~~temporal and spatial~~ patterns (Gelaro et al., 2017). The dust column mass density ~~was~~ is used to represent the atmospheric DA concentration under the MERRA-2 product during ~~the~~ 1980-2020 ~~period~~ (horizontal resolution: $0.625° \times 0.5°$) in this paper. Yao et al. (2021) used the MERRA-2 dataset to analyse the monthly mean DAs in China and found that ~~the DAs from March to July showed higher values with obvious variabilities, which~~the result was consistent with the previous conclusions obtained using different DA datasets (Che et al., 2019; Liu et al., 2020), demonstrating the feasibility and applicability of the MERRA-2 dataset for assessing the DAs in China.

The Sea Surface Temperature (SST) dataset was obtained from the Extended Reconstructed Sea Surface Temperature, version 5 (ERSST-5), from the National Oceanic and Atmospheric Administration (NOAA) ~~for~~ over the period 1980-2020 (horizontal resolution: $2.0° \times 2.0°$) (Huang et al., 2017). ~~The atmospheric reanalysis datasets, including the wind field, geopotential height field, sea level pressure field, temperature field, and vertical velocity field, were obtained from the European Center for Medium-Range Weather Forecasts, version 5 (ERA-5), over the period 1980-2020 (horizontal resolution: $0.25° \times 0.25°$). Compared to its predecessor, ERA-Interim, ERA5 has a modified data assimilation system and improved physical model to achieve reanalysis data information with improved quality.~~ The atmospheric reanalysis dataset, including the wind field, geopotential height field, sea level pressure field, temperature field, and vertical velocity field, obtained from the European Center for Medium-Range Weather Forecasts (ECMWF) is the fifth-generation reanalysis global atmosphere (ERA5) data set over the period 1980-2020 (horizontal resolution: $0.25° \times 0.25°$). Compared to its predecessor, ERA-Interim, ERA5 has a modified data assimilation system and improved physical model to achieve reanalysis data information with improved quality (Hersbach et al., 2020). In this paper, unless otherwise specified, the boreal winter season is referred to as December-January-February (DJF), and the spring season is March-April-May (MAM).

2.2 Methods

The NAO index (NAOI) was chosen to indicate the NAO activities. The NAOI describes the large-scale circulation characteristics of the NAO well (Li and Wang, 2003), and is defined by the following equation:

$$NAOI = \hat{P}_{35°N} - \hat{P}_{65°N} \tag{1}$$

In the above equation, P represents the monthly mean sea level pressure averaged from 80°W to 30°E, $\hat{P}$ is the standardized value of P, and the subscript $\hat{P}$ indicates the latitude. The selection criteria for the NAO abnormal years is based on the NAOI index averaged over the winter months, the index is then normalized, and the years with a NAOI exceeding 0.5 standard deviations are recorded as NAO anomalous years.

According to the operational criteria of the CNMC, DE occurrences are defined as when the

number of sites with DEs is more than 1/3 of the total amount in the selected region. According to

the variations in DAs and to assure the feasibility of DE sample number, we defined a DE when any

of three types of DEs occur. Although the DEs last for a short period of time, even only one day, the

abnormal atmospheric circulation that affects the DEs will exist over a long period before and after

the day of the outbreak of DEs (Li et al., 2022). Therefore, to investigate the abnormal atmospheric

signals during DEs, the time-scale was separated into the following parts: "Day -n", "Day 0" and

"Day +n", which indicate ~~previous~~prior to, the date of, and lag after the day of DE outbreak,

respectively. To probe obvious signals in DEs, we extended the number of days of DE cycle to 6

days, i.e., before the DE outbreak to "Day -3" and after the DE outbreak to "Day +2".

To analyse the features of transient eddy flux transport during DEs based on atmospheric

variables, the method of physical decomposition was used in this work (Qian, 2012). Any

atmospheric elements F, such as u, v, and T, can be decomposed into two parts according to the

above decomposition principle: the temporal mean part $\bar{F}$ and the transient eddy part F'. $\bar{F}$

represents the state in which the radiation from the subsurface at a fixed point in the atmosphere is

in equilibrium with the daily and annual cycles of solar radiation, while F' is a deviation from

the balanced state as follows:

$$F = \bar{F} + F' \tag{2}$$

In this paper, the transient eddy flux transport is denoted by $[u'v']$ and $[v'T']$, representing the

momentum and heat of transient eddy transport, respectively. Within the range of longitude that we

choose, the zonal means are represented in the variables by square brackets ([ ]).

3 Results

3.1 Selection of the dust aerosol study area and association with the NAO

The concentration of spring DA and their standard deviation distributions in China are shown

in Fig. 1. The large values of DAs are mostly situated in source regions such as Xinjiang and Inner

Mongolia. In addition, the DA concentrations in the non-dust source areas, north of the Yangtze

River (30°-40°N, 105°-120°E), also show high values (Fig. 1a).; that is, the spring DAs show higher

concentrations here than in other regions of China. Moreover, the standard deviation of DAs in this

region is also characterized as a large value, indicating that DAs have strong annual variability and

258 are easily influenced by dust disasters (Fig. 1b). Therefore, the area spanning (30°-40°N, 105°-

259 120°E) is selected as the study region to explore the variability of DAs and the possible formation

260 causes of DEs, which in the analysis that follows is referred to as North China.
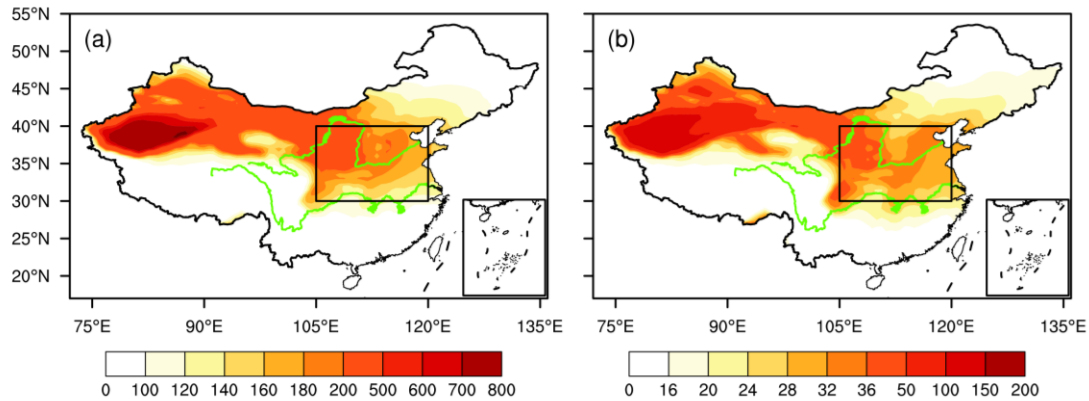
262 **Figure 1**. (a) Spatial distribution of the climatological spring dust column mass density and (b) dust
263 column mass density standard deviation, unit: mg m^{-2}. The black box indicates the North China.

264 To explore the possible links affecting the spring DAs in North China, the correlation

265 coefficients between the regional average DAs and the geopotential height field are illustrated in

266 the previous and contemporaneous periods (Fig. 2). The pattern of the MAM DAs and the DJF, JFM,

267 FMA and MAM geopotential height fields all show significant north–south reversal in the North

268 Atlantic, i.e., negative in the Azores and positive in Iceland, which indicates typical characteristics

269 of the NAO negative phase. This dipole structure can be observed in the lower, middle and upper

270 troposphere, denoting that there is an important connection between the spring DAs in North China

271 and the previous NAO variations. Furthermore, significant correlation coefficients can be found

272 between the spring DAs in North China and the NAOI in previous DJF, JFM, and FMA, and the

273 correlation coefficients are -0.39, -0.40, -0.40, -0.28, respectively~~Furthermore, significant~~

274 ~~correlation coefficients can be found between the spring DAs in North China and the NAOI in~~

275 ~~previous DJF, JFM, and FMA in the early period, and the correlation coefficients are all~~

276 ~~approximately -0.40~~. Simultaneously, as illustrated in Fig. 3, March, April and May, corresponding

277 to the spring months, show substantial standard deviations, suggesting that the DAs in North China

278 vary dramatically in these 3 months, while the monthly average standard deviations of the NAOI

279 present the highest values in December, January and February, corresponding to the winter.

280 Therefore, the effect of the NAO in boreal winter on the later spring DAs in North China and the

281 synoptic formation mechanism of the impact should be analysed and explored. Considering the

282 significant negative effect of the NAO on the DAs in North China, the main focus in the subsequent

283 analysis is on the negative phase of the NAO.

284
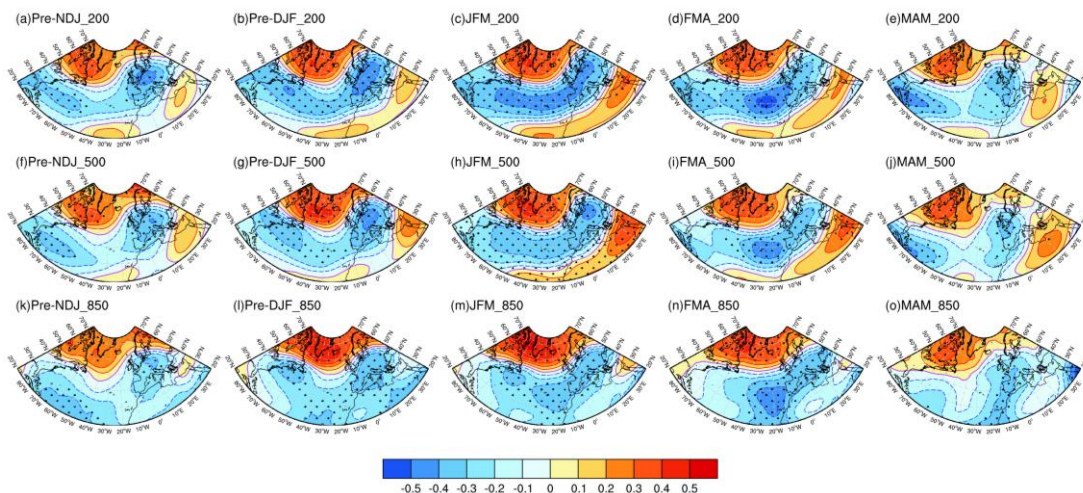
Figure 2. (a-e) Correlations of the spring dust column mass density in North China with geopotential height anomalies at 200 hPa during the previous and simultaneous seasons. (f-j) and (k-o), As in (a-e), but for the correlations with geopotential height anomalies at 500 hPa and 850 hPa, respectively. Dotted blue, solid magenta and solid red lines indicate negative, zero and positive contour values, respectively. The contour intervals are 0.1. The black dotted areas are significant at the 90% confidence level.

291
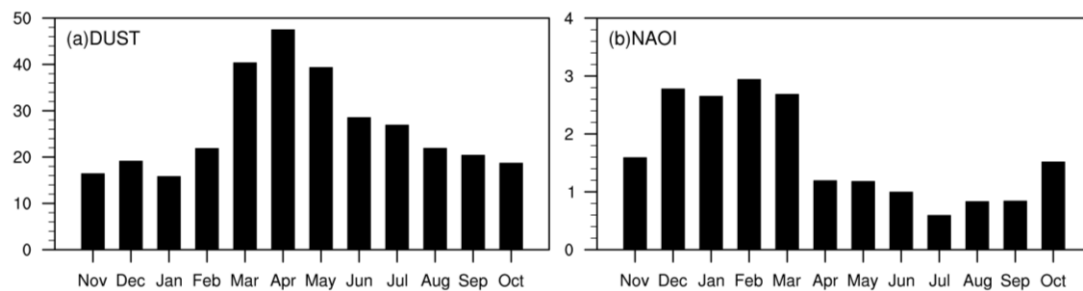
Figure 3. The monthly standard deviation of (a) the dust column mass density in North China and the (b) NAOI. The unit in (a) is mg m^{-2}.

294   According to the analysis, the NAOI in boreal winter and late spring DAs in North China have

295 a substantial negative link. How does the boreal winter NAO affect the late spring DAs in North

296 China? There is an obvious correlation between the boreal winter NAOI and both contemporaneous

297 and late North Atlantic SST anomalies (SSTA), as well as a triple-pole model of "-, +, -" (Fig. 4a to

298 b). Previous studies have noted that on seasonal and annual scales, the triple-pole of SST is the

299 primary mode of North Atlantic SST variation, and its variability is closely correlated to the changes

in the NAO (Wu et al., 2009). The NAO can modify SST by influencing changes in sea surface

wind speed and hence latent heat fluxes in the North Atlantic (Cayan et al., 1992). Simultaneously,

the triple-pole SST mode generates atmospheric circulation similar to the NAO, suggesting a

positive feedback between them, which has been verified in both observational data analysis (Czaja

et al., 2002) and ocean-atmosphere coupled model simulations (Watanabe et al., 2000). These

findings show that the SST has a "capacitor effect" on the NAO negative signal, which prolongs the

influence of the NAO signal over the surrounding and downstream areas. Moreover, through the

correlation distribution between the boreal winter NAOI and both contemporaneous and late North

Atlantic SSTA corresponding to the selected NAO negative phase years (1979, 1981, 1984, 1985,

1986, 1995, 1997, 2000, 2002, 2003, 2005, 2009, 2010, and 2012), it can be found that the North

Atlantic SSTA from boreal winter to late spring is manifested as a "-, +, -" triple-pole pattern

characteristic (Fig. 4c to d), which further verifies that the early NAO negative signal can be stored

in the North Atlantic SST and has an influence on the subsequent weather-climate over the

surrounding and downstream regions.
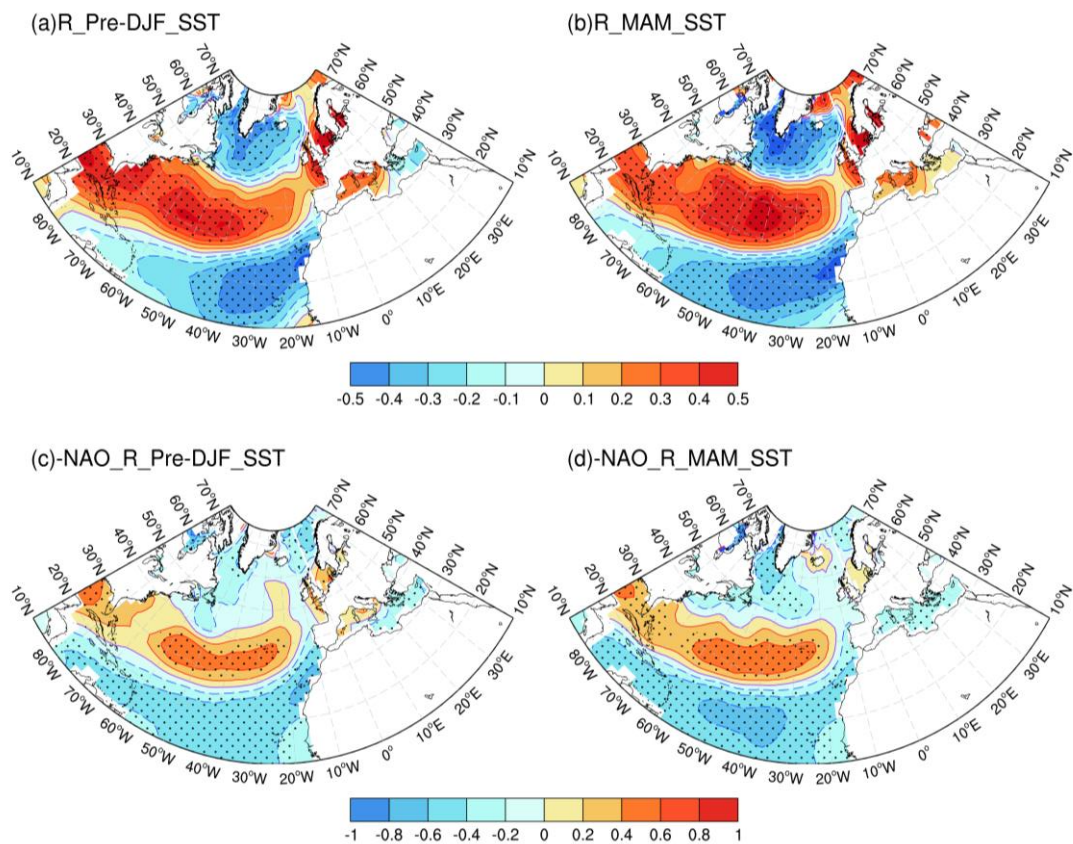
Figure 4. Correlations of the boreal winter NAOI with the (a) simultaneous and (b) following spring
SSTA. (c-d) As in (a-b), but during the negative NAO phases (1979, 1981, 1984, 1985, 1986, 1995,

317 1997, 2000, 2002, 2003, 2005, 2009, 2010, and 2012). Dotted blue, solid magenta and solid red
318 lines indicate negative, zero and positive values, respectively. The contour intervals are 0.1 in (a-b)
319 and 0.2 in (c-d). The black dotted areas are significant at the 95% confidence level.

3.2 Atmospheric circulation evolution during DEs

In this paper, we select 27 spring DEs in North China during the period of 1980-2020 based on the selection criteria, which are distributed over 17 years (Table. 1). It is found that there are shifts of the NAO from a positive to negative phase preceding all the DEs, highlighting the significant influence of the NAO negative phase on the occurrence of DEs. Among these, the 9 DEs (19800419, 19820408, 19820502, 19820508, 19850403, 19870317, 19980416, 20100320, 20130309) are striking based on the preliminary unusually strong winter NAO negative signal compared to that before the rest of DEs. At the climate-scale, the NAO intensity in boreal winter of the 9 DEs are all less than -0.5 standard deviations, which corresponds to the NAO negative phase years (Figure. 5a). Further analysis on the weather-scale indicates that the number of days with NAO negative phase (the value of NAOI less than -0.5) are above 35 days in the 3 months of boreal winter in the 9 DEs (Figure. 5b). Furthermore, the NAO negative phase is longer and more intense during these 9 DEs, while the NAO negative phase days in the remaining DEs are below 35 days (figure not shown). Therefore, to avoid information filtering caused by too many study cases and to reflect the statistical significance for studying the modulation effect of the NAO negative signal on the DEs in North China to the maximum extent, we chose these 9 DEs with the strongest influence of the NAO negative signal to study the evolution characteristics and synoptic causes of DEs in North China.

Table 1. Based on the CNMC selection criteria, 27 DEs and the years in which these DEs occurred

Years	DEs
1980, 1981, 1982, 1983, 1984, 1985	19800419, 19810308, 19810325, 19810502, 19820408, 19820502, 19820508, 19830316, 19830401, 19830428, 19840301, 19840420, 19840428, 19850403
1987, 1988, 1990, 1992, 1993, 1995	19870317, 19880411, 19880417, 19900407, 19920411, 19930424, 19950311
1998, 2000, 2002, 2010, 2013	19980416, 20000327, 20000409, 20020320, 20100320, 20130309

338
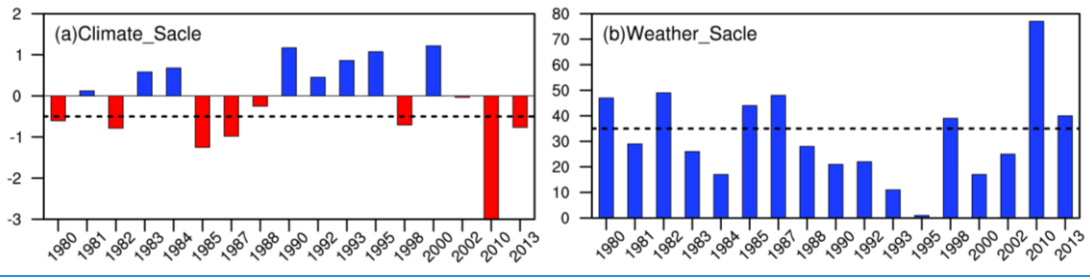
Figure 5. (a) The standardized inter-annual variability of the previous winter NAOI of the years in which these DEs occurred, (b) the number of days when the value of previous winter NAOI is less than -0.5 of the years in which these DEs occurred.

From the abnormal field of the spatial distribution of DA concentration synthesized by the selected DEs (Fig. 6), it can be found that before the outbreak of DEs, the positive anomalies of DA concentrations appear in the source regions (Xinjiang and Mongolia), and on "Day -1", the positive anomalous field gradually expands and develops into a positive anomaly belt with maximum values of 180 mg m^{-2}. At this time, the DA concentrations on the north side of North China already show obvious positive anomalies, providing sufficient source contributions for the next outbreak of DEs. On "Day 0", the overall DA concentration anomaly value exceeds 180 mg m^{-2} in North China, indicating that large-scale DEs have broken out. After the outbreak of DEs, the positive DA concentration anomalies in North China decrease rapidly, and the impact of DAs from Xinjiang and Mongolia on North China gradually weakens. Before the outbreak of DEs, the DA concentrations in Mongolia and Xinjiang, which are the primary source areas of DAs in East Asia (Zhang et al., 2003), gradually increase. In the growth process of DA concentrations, DAs are gradually transported eastward to North China. Therefore, the outbreak of DEs in North China is mainly caused by the rapid increase in DA concentrations and their eastward transmission from Xinjiang and Mongolia.
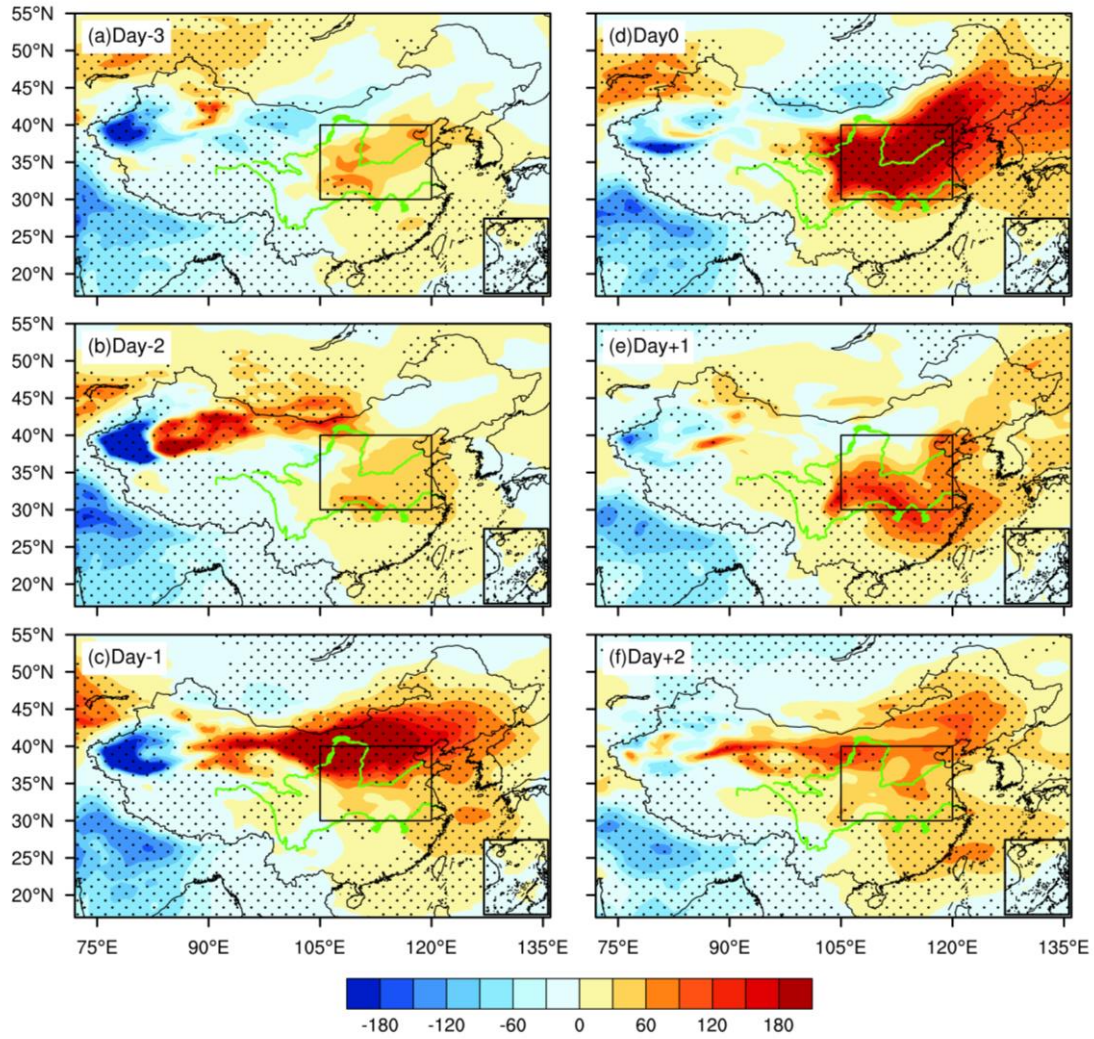
Figure 6. Spatial distribution of the dust column mass density anomalies in East Asia from "Day -3" to "Day +2" during DEs, unit: mg·m^{-2}. The black dotted areas are significant at the 95% confidence level.

The evolution of the 200 hPa atmospheric circulation during DEs is illustrated in Fig. 7~~6~~, representing features of the wind field in high levels of the troposphere. On "Day -3", there are large-scale anomalous positive zonal winds in the Siberian area, with positive zonal wind anomalies of +9 m s^{-1}. From "Day -2" to "Day -1", the positive zonal wind anomalies move southward, controlling the upstream area of North China (35°-50°N, 70°-110°E), as well as the ~~desert~~ dust source areas of Xinjiang and Mongolia. The zonal wind anomalies over the area of North China are in a "+, -, +" triple-pole pattern from the equator to 60°N, indicating that the boreal winter NAO negative signal can propagate to East Asia, resulting in changes in the East Asian subtropical jet stream (EASJS) and polar-front jet stream (PFJS) in late spring. In earlier investigations, similar

findings were noted (Shao and Zhang, 2012). ~~. For example, Shao and Zhang (2012) indicated that when the NAO is unusually strong (weak) in winter, the EASJS will strengthen (weaken) and the PFJS will weaken (strengthen).~~ There are also remarkable features of the EASJS along 30 °N, with two centres: the west centre is in northern Africa, with a central intensity of 40 m s^{-1}, and the east centre is situated in the western Pacific south of Japan, with a central intensity of 50 m s^{-1}. As a result of its far distance from the DA source regions in East Asia and North China, the western centre of the EASJS has a very limited impact on these regions. From "Day -3" to "Day -1", the eastern centre of the EASJS moves eastward, which leads to diminishing zonal winds at 200 hPa in North China, and the negative anomaly centre is lower than -9 m s^{-1}. From "Day 0" to "Day +2", the eastern centre of the EASJS stops moving eastward and recedes slightly westward, and the zonal winds over North China change to -6 m s^{-1}. Under the impact of the jet stream, there are anomalous positive zonal winds and negative zonal winds controlling the dust source areas of Xinjiang, Mongolia and North China, respectively. Through the effect of vertical circulation, abnormal winds at high altitudes can influence middle and low altitude winds through momentum compensation and downward (Li et al., 2015; Wu et al., 2016). Therefore, which may lead to the generation of windy weather near the DA source areas and the maintaining the DA concentration in North China, both of which contribute to the occurrence of DEs in North China.
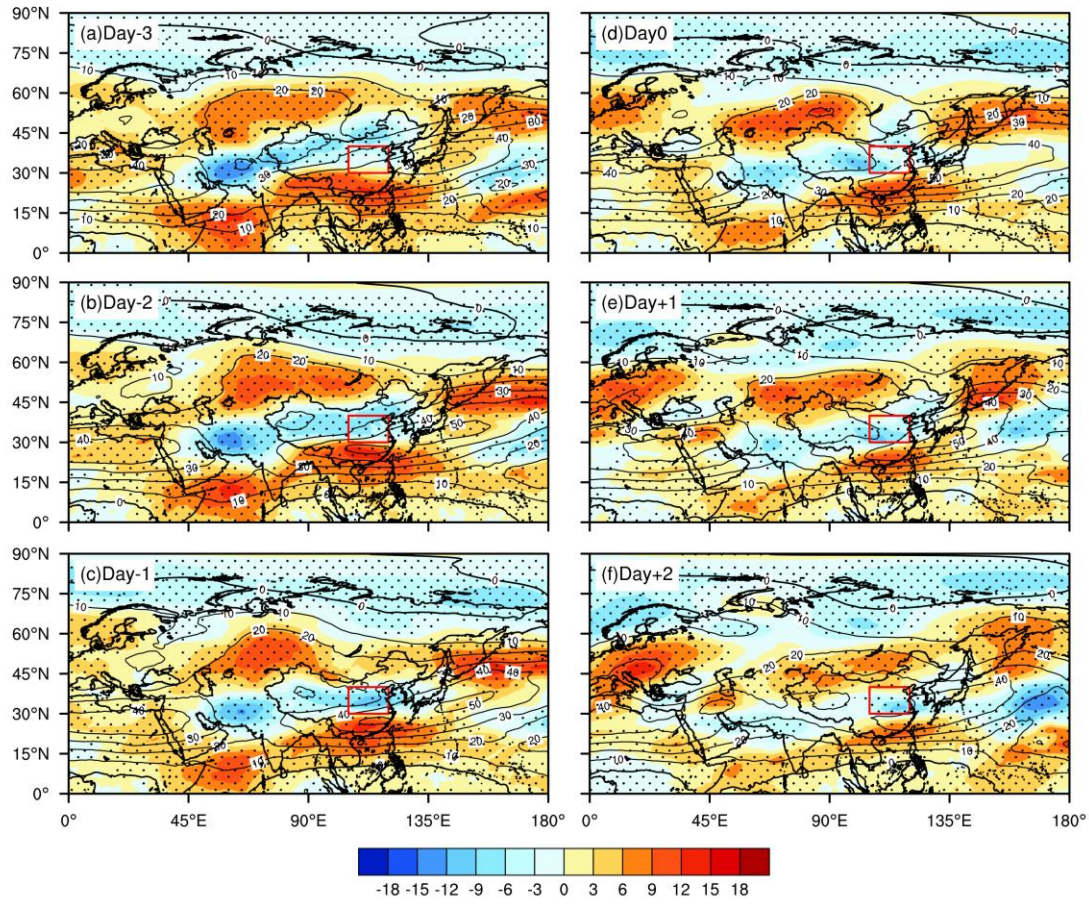
Figure 7. Spatial distribution of the 200 hPa winds (contour, unit: m s⁻¹) and their anomalies (shades, unit: m s⁻¹) from "Day -3" to "Day +2" during DEs. The black dotted areas are significant at the 95% confidence level.

To further determine the impact of the upper-level wind speed on the middle-lower wind speed, the vertical pressure-latitude distribution of the mean zonal winds and the vertical winds are calculated over the DA source areas and North China (Fig. 87). As shown in Fig. 87a to f, before the outbreak of DEs, due to the downward momentum of the zonal winds at high altitudes above the DA source areas, the enhancement of the wind speed in the middle-low levels is evident (Wu et al., 2016), resulting in the generation of strong surface wind to meet the dynamic conditions for the uplift of local DAs. After the outbreak of DEs, the average zonal winds in the high levels and the downward momentum effect weaken in DA source areas. Compared with the mean zonal winds in the troposphere over North China (Fig. 87g to l), from "Day -3" to "Day -1", corresponding to the weakening of the zonal winds in the high levels, the zonal wind speed in the middle-low levels decreases due to momentum compensation for the zonal winds in the high levels (Li et al., 2015),

402 which is conducive to the maintenance of DA concentration that is transported before the DE

403 outbreak, as well as in preparation for the subsequent DE outbreak in North China. After the DE

404 outbreak, the zonal winds at high altitudes on the north side of North China strengthen due to the

405 increase in zonal winds in the middle-low levels, and the DA concentration begins to decrease under

406 the effect of strong winds near the surface. It is also noted that during the whole evolution of DEs,

407 the south side of North China is dominated by southerly winds, which have a certain blocking effect

408 on the northward airflow carrying DAs and are favorable for maintaining the DA concentration in

409 North China.

410
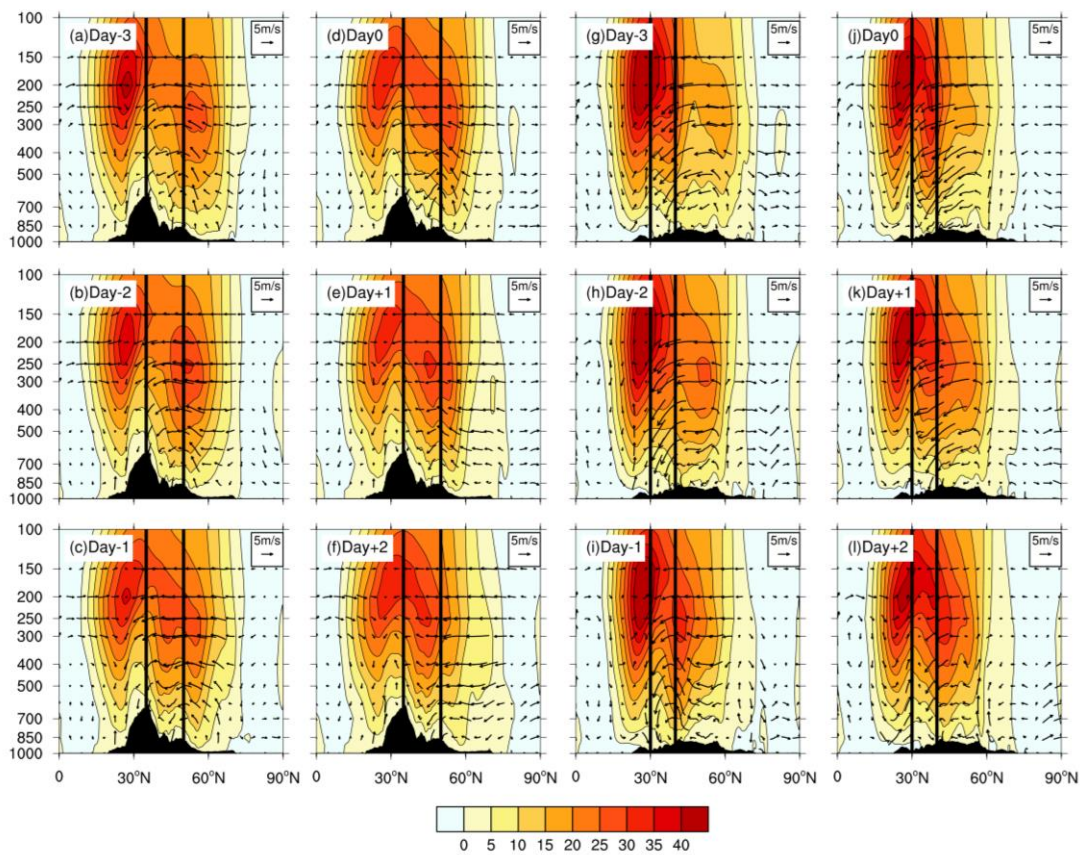
Figure 8. (a-f) Pressure-latitude section of zonal wind [u] (shaded, unit: m s^{-1}) and vertical wind
(arrow, (v, w), w expands 100 times, unit: m s^{-1}) averaged over 70°-110°E from "Day -3" to "Day
+2" during DEs. The area surrounded by the black line is the range of the source regions of DA. (g-
l) As in (a-f), but averaged over 105°-120°E.

415   In the evolution of atmospheric circulation of DEs at 500 hPa (Fig. 9~~8~~a to c), the trough-ridge

416 situation is characterized by two troughs and one ridge throughout the middle-high latitudes of the

417 Eurasian continent from "Day -3" to "Day -1". The two troughs are located in the Black Sea (~~20°~~

50 E, 30°-60°N, 20°-50°E) and the eastern part of Russia (~~105°-130°E,~~ 30°-60°N, 105°-130°E),

and the ridge is situated in the Ural Mountains (~~60°-80°E,~~ 25°-45°N, 60°-80°E). The western and

eastern troughs both show negative variations before the outbreak of DEs, with maximum values of

"-4 dagpm" and "-10 dagpm", respectively, while the Ural ~~ridge~~ Ridge (UR) manifests as gradual

enhancement with maximum values of "+6 dagpm". From "Day 0" to "Day +2", the intensities of

the trough and ridge all gradually weaken (Fig. 9~~8~~d to f). Before the outbreak of DEs, on account

of the strengthening advancement of the trough-ridge situation, the middle-high latitudes are

dominated by the strong meridional circulation, the transport of northern cold air ~~transport~~ increases,

and the southward invasion of the cold air enhances the local surface wind speed, leading to the

uplift of DAs in the DA source areas. After the outbreak of DEs, due to the changes in the trough-

ridge situation and the weakening of the UR, the cold air transport weakens. It should be noted that

the UR during DEs is much less than a blocking high based on the intensity as well as the duration.

The UR is established on "Day -1" and disappears basically on "Day +1", which is also consistent

with the feature that the maximum duration of DEs does not exceed 2 days (Li et al., 2022).
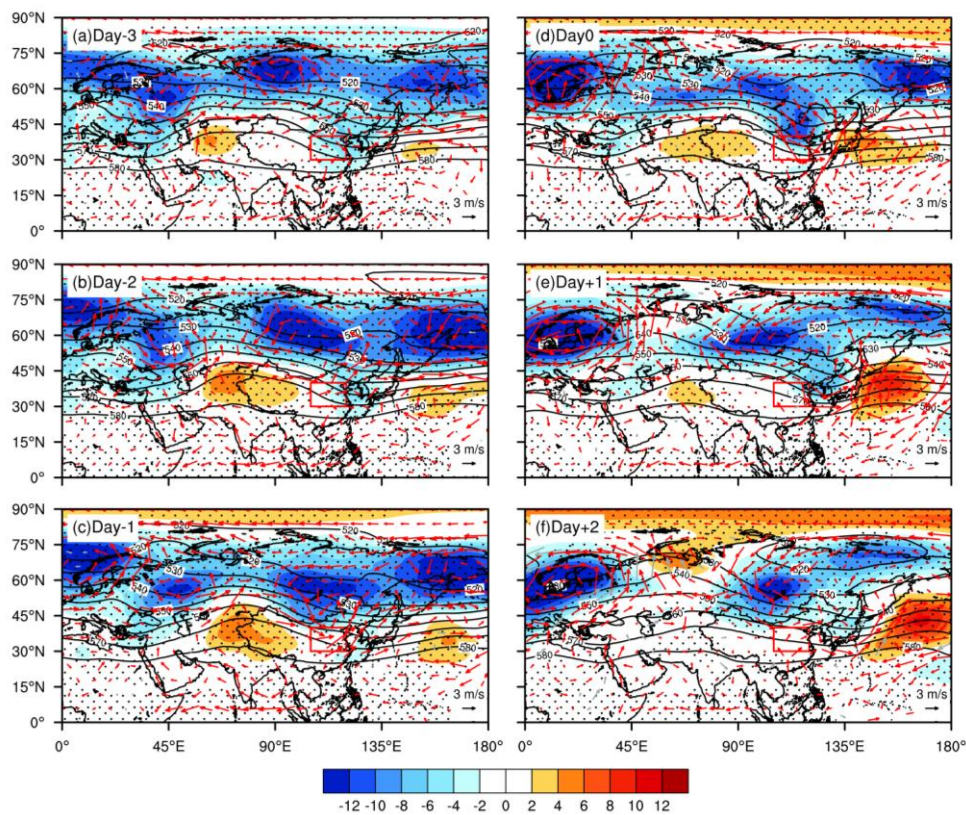
Figure 9. The spatial distribution of 500 hPa geopotential height (contour, unit: dagpm) overlays its
anomalies (shades, unit: dagpm) and 850 hPa wind anomalies (arrows, unit: m s^{-1}) from "Day -3"
to "Day +2" during DEs. The black dotted areas and red arrow areas are significant at the 95%

confidence level.

There is also a corresponding signal during DEs in the sea level pressure field (Fig. 109). On "Day -3", North China is controlled by an anticyclonic system dominated by sinking airflow. Therefore, poor precipitation conditions lead to the weak wet-deposition of DAs during transport (Kutiel and Furman, 2003). Meanwhile, the SH starts to appear in the upstream areas of North China. On "Day -2", the intensity of the SH is enhanced, with maximum values of "+6 hPa", and moves toward North China, while the intensity of the anticyclonic system controlling North China slightly weakens, and its position does not change significantly. In Mongolia, the MC starts to develop, accompanied by strong winds and vertical upward flows induced by the MC, which is conducive to the dynamic circumstances for the development uplift of DAs. On "Day -1", the location and intensity of the SH both change little, while the intensity of the anticyclonic system controlling North China weakens and even tends to disappear, and the intensity of the MC increases and moves slightly southward. On "Day 0", the SH moves eastward to the territory of Mongolia, and the MC moves southeastward, which is conducive to the transport of DAs from Mongolia to North China. From "Day +1" to "Day +2", the intensities of both the SH and MC start to weaken, and the impact on North China begins to weaken. In summary, under the negative phase of the NAO, before the outbreak of DEs, due to the establishment, strengthening and southward movement of the SH and MC, there is a wide range of northerly winds and the outbreak of cold air to the south, which is advantageous for the uplift and transmission of DAs to North China. Simultaneously, North China is controlled by an anticyclonic system, leading to local weather, mainly sunny conditions and weak winds, which is also favorable for the transport of DAs to North China. After the outbreak of DEs, both the SH and MC start to weaken, indicating that the uplift of DAs in the DA source areas and the dust transmission activities to North China start to weaken.

From the above atmospheric circulation characteristics, under the NAO negative phase, the crucial synoptic systems leading to DE occurrences in North China are the abnormal winds by the anomalies of the upper-level EASJS, the UR, the SH and the frontal cyclone (MC) near the surface. In addition, transient eddy is crucial for the abnormal evolution of atmospheric circulation. The mechanisms of the formation of these synoptic system anomalies from the view of transient eddy are investigated to reveal the mechanism of the synoptic cause for the DEs in North China under

465   the modulation of the NAO negative phase.

466
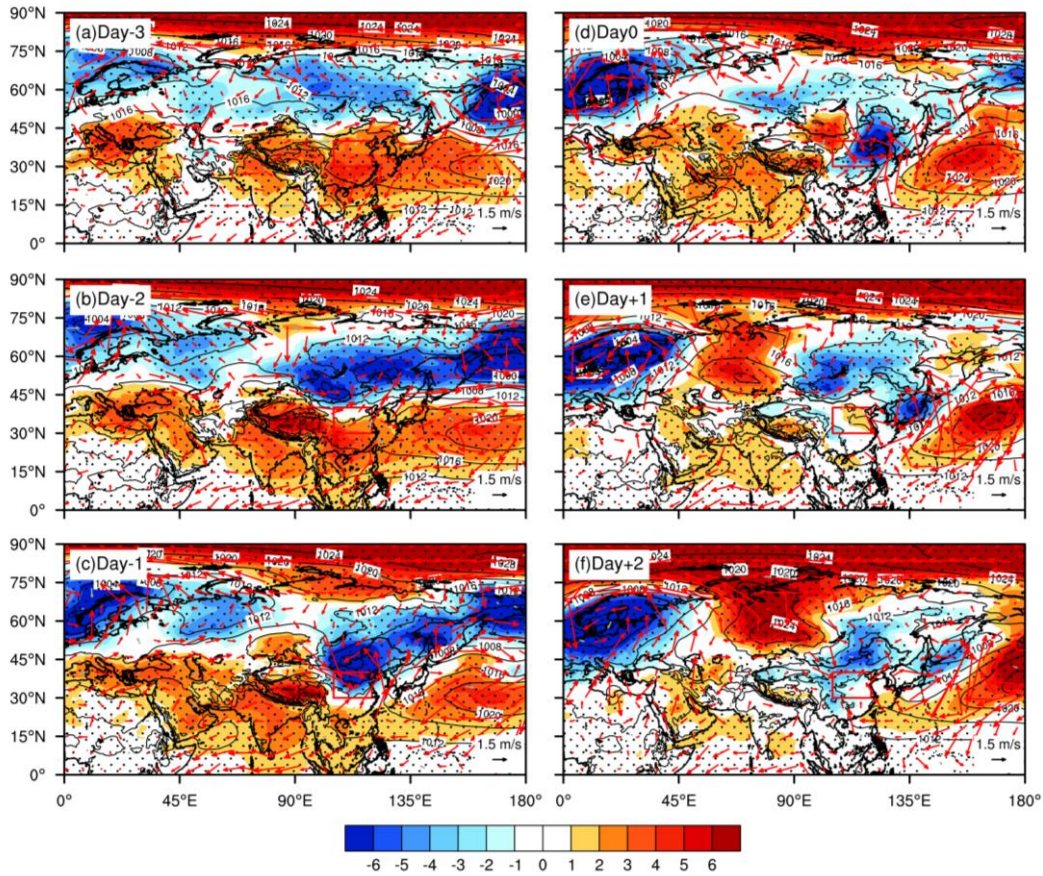
467 **Figure 10**. Spatial distribution of the sea level pressure (contour, unit: hPa) overlays its anomalies
468 (shades, unit: hPa) and 1000 hPa wind anomalies (arrows, unit: m s^{-1}) from "Day -3" to "Day +2"
469 during DEs. The black dotted areas and red arrow areas are significant at the 95% confidence level.

470 **3.3 Transient eddy flux transport characteristics during DEs**

471   Transient eddy fluctuations contribute to the maintenance of the atmospheric energy balance

472 through energy transport, and the energy transport process causes the divergence and convergence

473 of energy and mass between different regions, thus forming new regions of forcing within the

474 atmosphere (Li et al., 2019b). Transient eddy flux transport can enhance the positive pressure

475 component of the mean airflow and compensate for ground friction, which has a significant effect

476 on the maintenance of atmospheric circulation. For example, transient eddy momentum transport is

477 associated with the development of blocking high generation, and momentum transport contributes

478 differently during each period of its development (Li et al., 2019b). DE occurrences are inevitably

479 accompanied by tropospheric atmospheric circulation anomalies, and transient eddy flux transport

480 plays a significant role in the process of atmospheric circulation. Therefore, the possible

481 mechanisms of transient eddy momentum and heat transport during DEs under the NAO negative

482 phase on the change in major synoptic system anomalies are further analysed and explored.

483   The "+" ("-") sign of $[u'v']$ implies the poleward (equatorward) transport of transient eddy

484 momentum, and the "+" ("-") sign of $[u']$ represents the positive (negative) anomaly of the zonal

485 winds. Analysing the transport features of transient eddy momentum within the active range of the

486 UR during DEs (Fig. 11a to f), it is found that a pattern of "positive south and negative north"

487 appears with poleward, equatorward momentum transport near 30°N and 40°N at approximately

488 200-500 hPa on "Day -3", respectively, while a $[u'v']$ convergence centre exists within the area of

489 the UR. On "Day -2", the feature of $[u'v']$ in the Urals region changes from convergence to

490 divergence, and on "Day -1", the "negative south and positive north" pattern of transient eddy

491 momentum reaches the highest value during DEs, with maximum values of -24 m^2 s^{-2} and +30 m^2 s^-

492 ^{2}, respectively. After the outbreak of DEs, the intensity of the $[u'v']$ centre in the Urals region rapidly

493 decreases, with no longer obvious $[u'v']$ transport. For the zonal wind anomalies $[u']$ (Fig. 11g to l),

494 before the outbreak of DEs, $[u']$ in the Urals region there is a "negative south and positive north"

495 mode, which is mainly controlled by negative $[u']$, with maximum values of -12 m s^{-1},

496 corresponding to divergence of $[u'v']$. From "Day 0" to "Day +1", the UR region gradually becomes

497 dominated by the "+" signal of $[u']$. On "Day +2", as there is unobvious $[u'v']$ within the region of

498 the UR, the intensity of $[u']$ weakens rapidly. Investigation of the transient eddy momentum

499 transport characteristics and the changes in the zonal wind anomalies during DEs show that there is

500 an obvious divergence centre of the transient eddy momentum within the range of UR before the

501 outbreak of DEs, corresponding to zonal wind weakening and the establishment of meridional

502 circulation. Therefore, transient eddy momentum transport has an indirect influence on the

503 establishment and advancement of the UR (Li et al., 2022). To obtain a better understanding of the

504 role of transient eddy momentum on anomalies of the wind field during DEs, the $[u'v']$

505 characteristics of the DA source areas are further analysed (Fig. 12a to f). The transient eddy

506 momentum pattern of "positive south and negative north" in the DA source areas is gradually

507 displayed at 200-500 hPa from "Day -3" to "Day -1", with maximum values of +36 m^2 s^{-2} and -36

508 m^2 s^{-2}, respectively. After the outbreak of DEs, the source areas of DAs are mainly controlled by

509 the weak $[u'v']$ negative centre, with unobvious transient eddy momentum. For the zonal wind

510   anomalies [u'] (Fig. 12g to l), before the outbreak of DEs, the DA source regions gradually become

511   dominated by positive [u'], with maximum values of +10 m s^{-1} on account of the convergence of

512   transient eddy momentum, facilitating the uplift of DAs. After the outbreak of DEs, [u'] still

513   predominantly increases, indicating that there are more complex reasons for the zonal wind changes

514   than the transport of transient eddy momentum, which deserves in-depth analysis later.

515
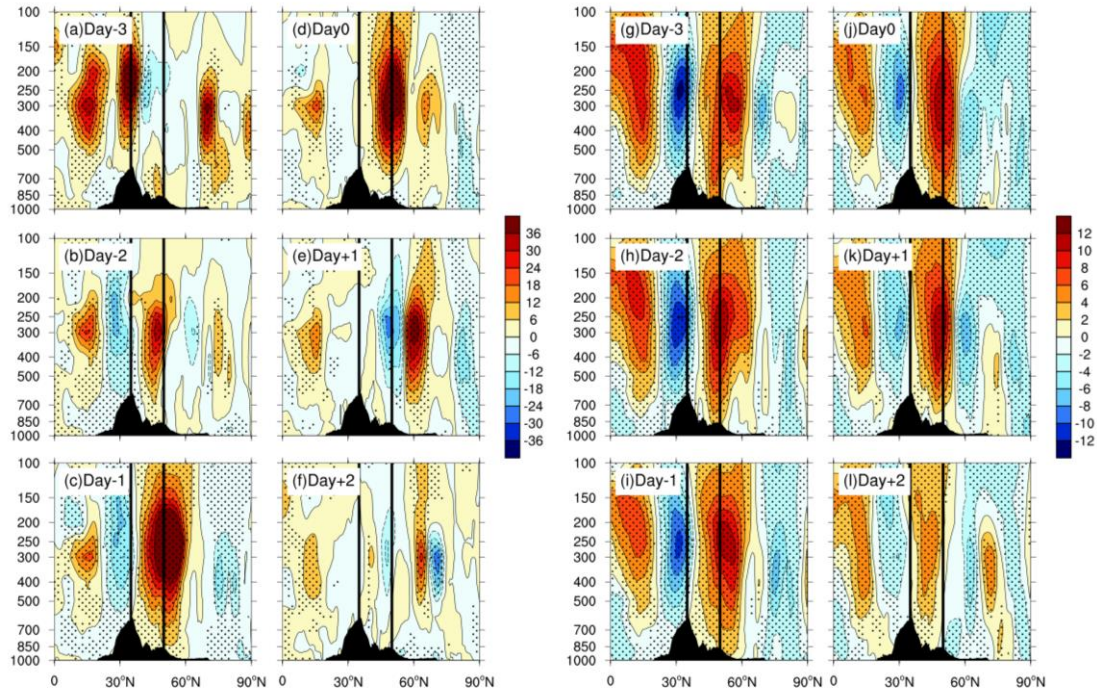
516 **Figure 11**. Pressure-latitude section of (a-f) the mean transient momentum [$u'v'$] (unit: m^2 s^{-2}) and
517 (g-l) zonal wind anomalies [u'] (unit: m s^{-1}) averaged over 60°-80°E from "Day -3" to "Day +2"
518 during DEs. The area surrounded by the black line is the range of the UR. The black dotted areas
519 are significant at the 95% confidence level.

Atmospheric circulation also heavily depends on transient eddy heat transport (Li et al., 2019b; Li et al., 2022). Similar to the features of transient eddy momentum transport, the "+" ("-") sign of $[v'T']$ describes the poleward (equatorward) transport of transient eddy heat, and the "+" ("-") sign of $[T']$ implies an increase (decrease) in temperature. In the analysis of the $[v'T']$ characteristics within the range of UR during DEs (Fig. 13a to f), it is found that the convergence of transient eddy heat is dominant at 200-500 hPa on "Day -3", with maximum values of +12 m·s^{-1}·K and -6 m s^{-1}·K, respectively. During the subsequent "Day -2" to "Day -1", the UR area is dominated by a strong positive $[v'T']$ centre, which also exhibits the convergence features of transient eddy heat. There are unobvious features of $[v'T']$ in the developmental range of the UR from "Day 0" to "Day +2". In the analysis of the temperature anomalies $[T']$ (Fig. 13g to l), it is shown that before the outbreak of DEs, the area with developed UR is in the convergence region of transient eddy heat, and $[T']$ becomes more visible when the transient eddy heat transport increases, showing a "negative south and positive north" pattern below 300 hPa. The temperature gradient $(-\partial T/\partial y)$ is weakened here by the thermal wind formula ($u_T = R \cdot -\frac{\partial T}{\partial y}$, where u_T, R, T demonstrate the thermal wind, gas

539   constant and temperature, respectively), and the thermal wind will be weakened due to the decline

540   in the temperature gradient. When the thermal wind is weakened, the zonal winds are also weakened,

541   which facilitates the establishment of meridional circulation and the development of a blocking

542   situation (Li et al., 2019b). After the outbreak of DEs, $[T']$ decreases due to the weakening of the

543   transient eddy heat transport. From "Day 0" to "Day +1", the negative $[T']$ anomaly centre appears

544   north of the UR, and the negative $[T']$ centre gradually moves southward, which corresponds to the

545   increase in the temperature gradient here and is not favorable to the development of the UR. The

546   transient eddy heat transport also has an impact on the wind field for the source regions of DAs (Fig.

547   14a to c). Before the outbreak of DEs, the $[v'T']$ over the DA source areas gradually evolves to be

548   dominated by the convergence above 300 hPa, while the divergence of $[v'T']$ is dominated below

549   300 hPa. The strongest $[v'T']$ convergence and divergence characteristics are both reached on "Day

550   -1". After the outbreak of DEs (Fig. 14d to f), the DA source regions are controlled by a positive

551     $[v'T']$ centre, with the convergence of $[v'T']$ on "Day 0". From "Day +1" to "Day +2", there are

552   unobvious $[v'T']$ features over the source areas of DAs. Analysis of the temperature anomalies $[T']$

553   (Fig. 14g to l) reveals that below 300 hPa in the DA source regions before the outbreak of DEs, the

554   transient eddy heat transport weakens with time due to the "positive south and negative north" mode

555   of $[T']$, with maximum values of +2 K and -2 K, respectively. The temperature gradient is enhanced,

556   and the development of thermal wind leads to the enhancement of zonal winds. In addition, the

557   zonal winds in the middle-low levels are enhanced by the enhanced thermal wind, and the

558   momentum downward transport of zonal winds in the high levels further enhances the zonal winds

559   in the middle-low levels, which is conducive to the uplift of DAs. In addition, the convergence of

560     $[v'T']$ is not favorable to the development of the zonal winds above 300 hPa according to the thermal

561   wind formula, which hinders the momentum downward transport of the zonal winds in the high

562   levels in the DA source areas. Transient momentum transport has a greater effect on the variability

563   of zonal winds at high levels than transient eddy heat transport (Solomon, 1997).
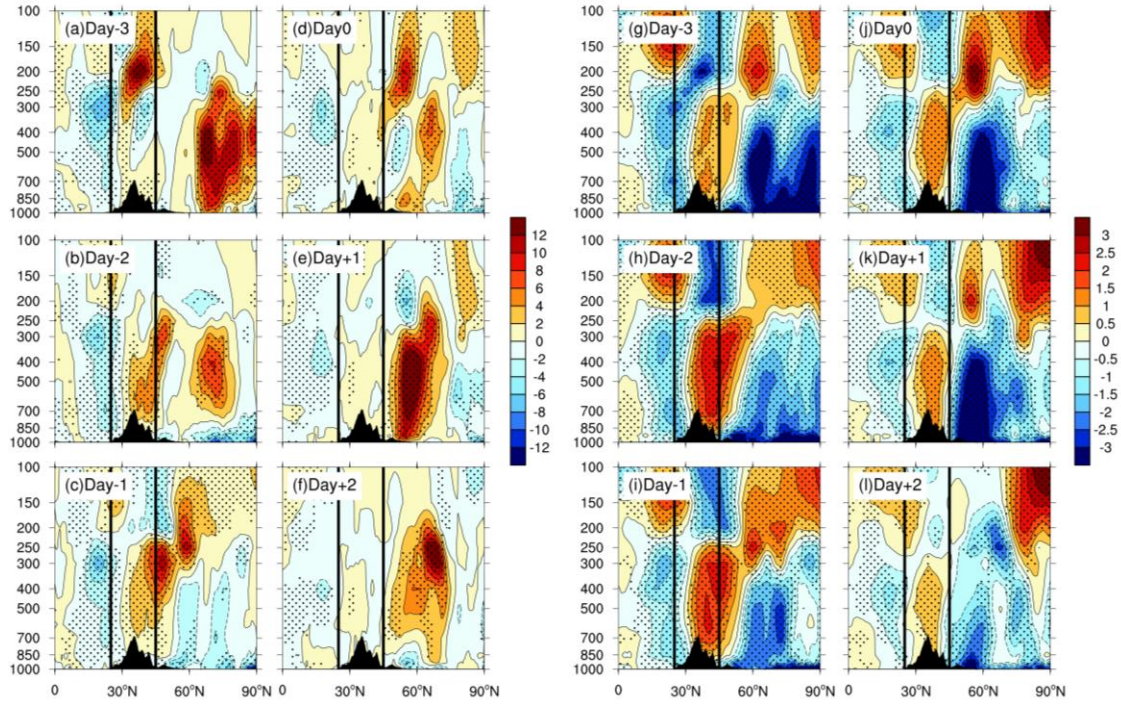
Figure 13. Pressure-latitude section of (a-f) the mean transient heat $[v'T']$ (unit: m s^{-1} K) and (g-l) temperature anomalies $[T']$ (unit: K) averaged over 60°-80°E from "Day -3" to "Day +2" during DEs. The area surrounded by the black line is the range of the UR. The black dotted areas are significant at the 95% confidence level.
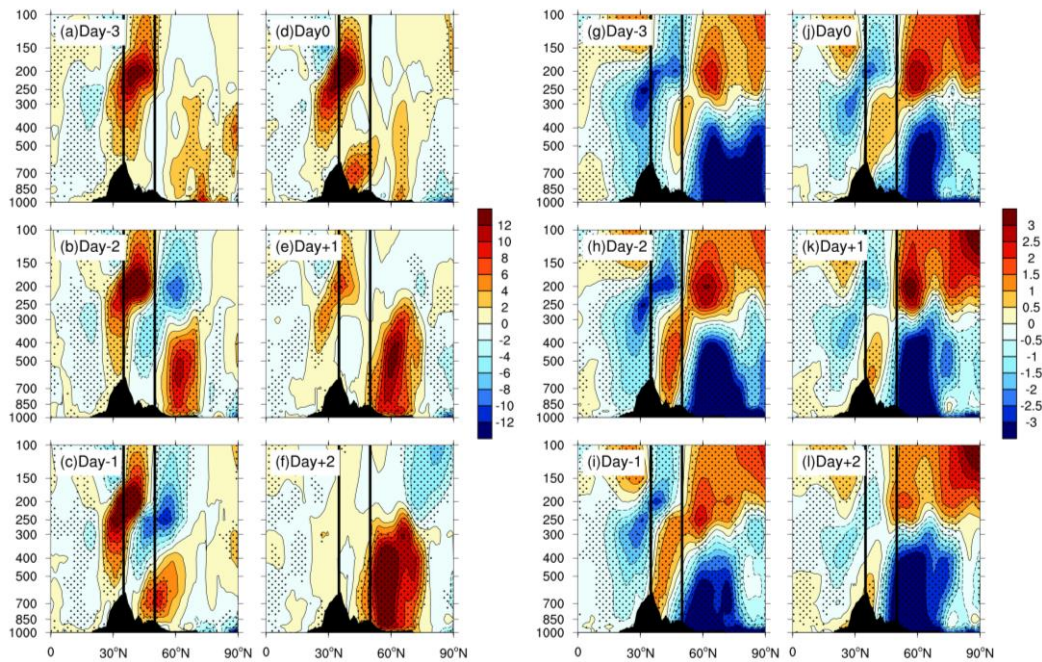
Figure 14. Pressure-latitude section of (a-f) the mean transient heat $[v'T']$ (unit: m s^{-1} K) and (g-l) temperature anomalies $[T']$ (unit: K) averaged over 70°-110°E from "Day -3" to "Day +2" during DEs. The area surrounded by the black line is the range of the source regions of DA. The black dotted areas are significant at the 95% confidence level.

574   The transient eddy flux transport characteristics during DEs show that the changes in $[u'v']$ and

575    $[v'T']$ in the DA source regions and the active range of the UR cause both energy and mass

576   divergence in North China, leading to diminishing zonal winds at high levels over North China

577   during DEs. Meanwhile, the zonal winds in the middle-low levels weaken through vertical

578   circulation due to the diminishing zonal winds at high levels, accompanied by southerly airflow on

579   the south side of North China, facilitating the maintenance of DA concentrations.

580   Results of the previous analysis of the transient eddy flux transport characteristics indicate that

581   the evolution of the UR may be explained by the divergence of transient eddy momentum and the

582   convergence of transient eddy heat by the thermal wind formula. By using the equation for the quasi-

583   geostrophic potential, this mechanism can also be verified (Gary, 2012~~1~~) as follows:

584
$$\left[\nabla^2 + \frac{\partial}{\partial p} \cdot \left(\frac{f^2}{\sigma} \cdot \frac{\partial}{\partial p}\right)\right] \cdot \frac{\partial \Phi}{\partial t} = -f \cdot \overrightarrow{V_g} \cdot \nabla(\xi_g + f) - \frac{\partial}{\partial p} \cdot \left[-\frac{f^2}{\sigma} \cdot \overrightarrow{V_g} \cdot \nabla\left(-\frac{\partial \Phi}{\partial p}\right)\right] \qquad (3)$$

585   Where $f, \Phi, \overrightarrow{V_g}$ denote the Coriolis parameter, geopotential height, and geopotential wind,

586   respectively, and $\sigma = -\frac{RT}{P} \cdot \frac{\partial \ln \theta}{\partial p}, \xi_g = \frac{\partial V_g}{\partial x} - \frac{\partial U_g}{\partial y} = \frac{1}{f} \cdot \nabla^2 \cdot \Phi$ denote the static stability and the

587   geostrophic relative vorticity, respectively. The first and second terms on the right-hand side of the

588   equal sign of Eq. (3) have the following equivalence after simplification:

589
$$-\frac{\partial \Phi}{\partial t} \propto -\overrightarrow{V_g} \cdot \nabla \xi_g \qquad (4)$$

590
$$\frac{\partial \Phi}{\partial t} \propto \frac{\partial}{\partial p}\left(-\overrightarrow{V_g} \cdot \nabla T\right) \qquad (5)$$

591   On the trough-ridge lines, since the vorticity advection in Eq. (4) is zero and the height of the

592   isobaric surface has no change, it only moves the ridges and does not change the strength of the

593   ridges. The temperature advection in Eq. (5) mainly acts on the trough-ridge lines, which affects the

594   development of the trough-ridge intensity but has no influence on its movement. In this study, we

595   mainly consider the change in trough-ridge intensity during DEs by noting the effect of temperature

596   advection. Temperature advection generally decreases with height, so it is sufficient to discuss only

597   the signs of positive and negative temperature advection here. Analysis of transient eddy heat

598   transport characteristics reveal that the transport of transient eddy heat in the UR region before the

599   outbreak of DEs will lead to uneven temperature distribution, which in turn leads to the development

600   of warm advection. The analysis of the quasi-geostrophic potential theory shows that the

601   development of warm advection in this region is beneficial to the development of the UR and to the

602   establishment of a temperature ridge. After the outbreak of DEs, the temperature advection starts to

603   weaken as $[v'T']$ no longer change within the area of UR, and thus, the intensity of UR also starts to

604   weaken.

605   Meanwhile, the active development of temperature advection and vorticity advection due to

606   transient eddy heat transport and the enhancement of UR, based on the Ω equation in the quasi-

607   geostrophic theory (Gary, 2012~~1~~), can also explain abnormal evolutions of the SH as well as the

608   MC near the surface during DEs, as follows:

$$\left(\nabla^2 + \frac{f^2}{\sigma} \cdot \frac{\partial^2}{\partial p^2}\right)\omega = \frac{f}{\sigma} \cdot \frac{\partial}{\partial p}\left[\overrightarrow{V_g} \cdot \nabla(\xi_g + f)\right] + \frac{1}{\sigma} \cdot \nabla^2\left[\overrightarrow{V_g} \cdot \nabla\left(-\frac{\partial \Phi}{\partial p}\right)\right] \tag{6}$$

610   Where $f, \omega, \Phi, \overrightarrow{V_g}$ denote the coriolis parameter, vertical velocity, geopotential height, and

611   geopotential wind, respectively, and $\sigma = -\frac{RT}{P} \cdot \frac{\partial \ln \theta}{\partial p}, \omega = \frac{dp}{dt}, \xi_g = \frac{\partial V_g}{\partial x} - \frac{\partial U_g}{\partial y} = \frac{1}{f} \cdot \nabla^2 \cdot \Phi$ and

612   denote the static stability, vertical velocity, and geostrophic relative vorticity, respectively. After

613   simplification, the first and second terms in Eq. (6) to the right of the equal sign are equivalent to

614   the following:

$$\omega \propto \frac{\partial}{\partial p} \cdot \left[-\overrightarrow{V_g} \cdot \nabla\xi_g\right] \tag{7}$$

$$\omega \propto \overrightarrow{V_g} \cdot \nabla T \tag{8}$$

617   According to Eq. (7) and (8), the relationship between the vertical velocity and vorticity

618   advection, temperature advection can be obtained, respectively. When the positive (negative)

619   vorticity advection increases with height, the degree of counterclockwise (clockwise) rotation

620   increases there, and the divergence (convergence) increases with height under the Coriolis force,

621   which will produce the rising (sinking) motion. As the vorticity advection generally increases with

622   height, it is sufficient to discuss only the signs of positive and negative vorticity advection here. In

623   short, it is expressed as warm (cold) advection corresponding to the rising (sinking) motion. Before

624   the outbreak of DEs, the northwest winds in front of the UR are strengthened along with the

625   enhancement of the ridge, and the northwest winds correspond to the development of negative

vorticity advection and cold advection. According to the quasi-geostrophic theory, a sinking motion will be generated in front of the UR, which corresponds to pressurization at the surface and will promote the establishment, strengthening, and southward movement of the SH. Similarly, the Mongolian region is located in front of the trough at this time, controlled by the southwest winds. Corresponding to the development of positive vorticity advection and warm advection here, an upward motion will be generated in Mongolia, corresponding to depressurization at the surface, which will promote the establishment, enhancement, and southward movement of MC there. After the outbreak of DEs, both the SH and MC start to weaken by reversal impacts of the temperature and vorticity advections due to the weakening of the trough-ridge situation at a deeper level due to the change in transient eddy transport conditions.

4 Conclusions and discussions

As a significant extra-equatorial mode of low-frequency atmospheric variability with a periodic signal on the seasonal-scale in the NH and a dominant mode of seasonal to annual winter semi-annual variability, the NAO has an influence on the DEs in East Asia, with significant regional characteristics. The spring DA concentration in North China, a non-dust source region, exhibits high values and strong annual variability. In this study, it is found that the boreal winter NAO negative signal has a significant effect on the DEs in late spring in North China. Modulated by the NAO negative signal, the tropospheric weather situation shows obvious anomalies, and the evolution mechanism can be revealed from the perspective of transient eddy transport. And we use the NAOI provided by Climate Prediction Center, which has been used in many studies (Zuo et al., 2015; Li et al., 2021a; Yao et al., 2022), for correlation analysis with the NAOI used in this work and find a good agreement with a correlation coefficient of 0.83 (figure not shown). This point indicates that the result would not be affected by choice of NAOI.

The boreal winter NAO negative signal through the "capacitor effect" of the North Atlantic prolongs its atmospheric signal and influences the late spring DEs in North China. Under the modulation impact of the upstream NAO negative signal, before the outbreak of DEs, the zonal winds at 200 hPa above the DA source regions gradually increase, and the increased zonal winds in the high levels transport the momentum to the zonal winds in the middle-low levels through the

vertical circulation, which is favorable to the uplift of DAs in the DA source areas. Meanwhile, the zonal wind in the high levels is dominated by negative anomalies over North China, which has a counter effect on the zonal winds in the middle-low levels by vertical circulation and facilitates the maintenance of DA concentrations in North China. At 500 hPa, the trough-ridge situation is obvious in Eurasia continent, the transport of northern cold air increases, and the southward invasion of the cold air enhances the local surface wind speed in the DA source areas, leading to the uplift of DAs. Near the surface, the SH and MC are established, enhanced and move southward, providing the northerly airflow in front of the DA source regions, guiding the cold air at high latitudes southward and acting favourably to the uplift and transmission of DAs to downstream North China. Simultaneously, the south side of North China is dominated by southerly winds, which have a blocking effect on the northerly airflow carrying DAs, facilitating the maintenance of DA concentrations in North China. After the outbreak of DEs, both favorable atmospheric circulations weaken gradually, and the DAs also start to decrease in North China.

Transient eddy has an important effect on the synoptic evolution of DEs through the modulation of the NAO negative signal. In advance of the outbreak of DEs, the transient eddy momentum at 300-500 hPa above the DA source region is dominated by convergence, and thus, the zonal winds are enhanced. Meanwhile, the characteristics of transient eddy heat over the source areas of DAs are mainly divergence, and the temperature anomalies are in a "positive south and negative north" pattern, resulting in enhancement of the temperature gradient and the zonal winds. Therefore, the zonal winds over the DA source regions increased by both the downward momentum and thermal wind, which is favorable to the uplift of DAs. Within the area of UR, the transient eddy momentum (heat) diverges (converges). The divergence of transient eddy momentum will lead to the weakening of zonal winds, while the decrease in zonal winds and the reduction in temperature gradients are both favoured by the convergence of transient eddy heat. The establishment and growth of the meridional circulation are significantly influenced by both, which is conducive to the development of the UR. The changes in upstream transient eddy flux transport cause both energy and mass divergence in North China, resulting in diminishing zonal winds during DEs, facilitating the maintenance of DA concentration. After the outbreak of DEs, the transient eddy flux transport characteristics in both the Ural region and the source areas of DAs gradually weaken, and the effect

683   on the zonal winds within these regions is also reduced.

684   In this study, we examine how the late spring DEs in North China are impacted by the boreal

685   winter NAO negative signal and the corresponding synoptic mechanism from the view of transient

686   eddy flux transport on the weather-scale by selecting 9 DEs from 1980 to 2020. Our focus is

687   different from previous analyses of the NAO and the DEs in China on the seasonal climate-scale

688   (Tang et al., 2005; Zhao et al., 2012). The findings demonstrate that the boreal winter NAO negative

689   signal can store its signal in the North Atlantic as a triple-pole structure of "-, +, -", which then

690   releases in late spring and affects the anomaly of atmospheric circulation in the troposphere by

691   transient eddy flux transport, as well as the zonal winds over the DA source regions and North China.

692   The thermal wind principle and the quasi-geostrophic theory can both explain this mechanism.

693   According to changes in the temperature gradient, the thermal wind principle directly explains

694   variations in the wind fields by the convergence and divergence of the thermal and momentum

695   transient eddy flux during DEs. The quasi-geostrophic theory can illustrate the abnormal formation

696   mechanism of synoptic systems in the whole troposphere during DEs. To be more precise, the

697   influence of the NAO negative signal in transient eddy fluxes causes temperature and vorticity

698   advection to develop; therefore, both mid-upper-level systems (the UR) and surface systems (the

699   SH and MC) strengthen, which can be explained by the height tendency equation and Ω equation,

700   respectively. The development of the above synoptic systems is favorable to the uplift of DAs in the

701   DA source areas and the transmission process to North China. Meanwhile, the southward airflow

702   on the south side of North China is favorable for maintaining the stable high value of DA

703   concentration for 1-2 days. The results are illustrated in Fig. 15, which displays the main synoptic

704   systems and transient eddy flux transport characteristics during DEs against the background of the

705   NAO negative phase. The result is helpful for a thorough comprehension of the mechanism

706   underlying the formation of DEs in eastern China and can serve as a point of reference for the

707   seasonal forecasting of DEs (Hong et al., 2019).
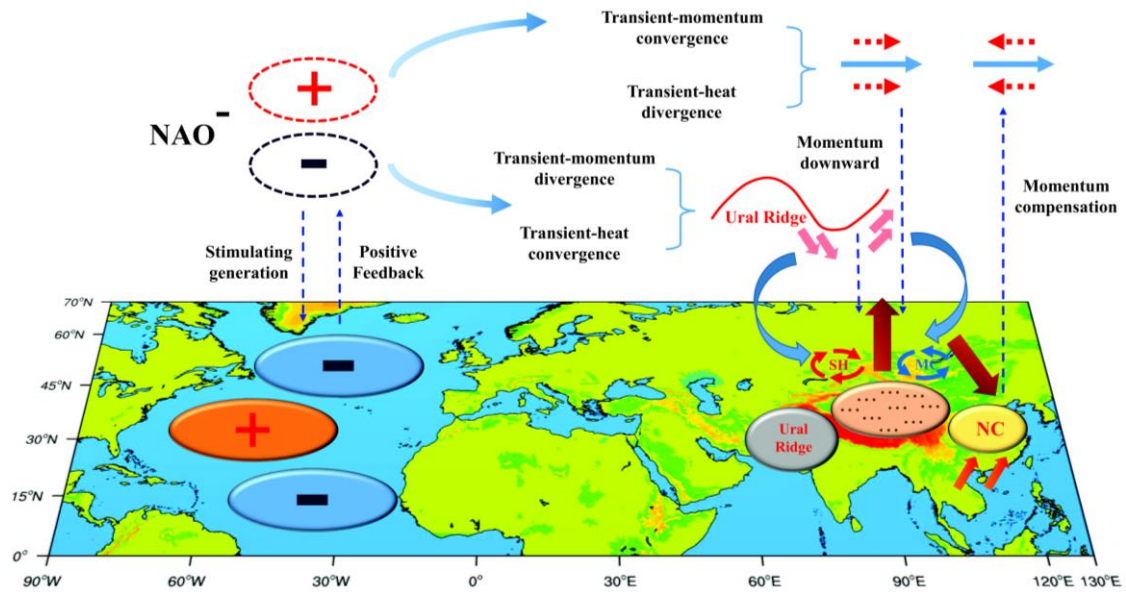
Figure 15. A schematic diagram of the main synoptic system anomalies and the role of transient eddy fluxes during DEs.

In addition to transient eddy, stationary eddy is also crucial in the development of atmospheric circulation, and the energy transport of stationary eddy differs from that of transient eddy, and has been applied to the analysis of atmospheric circulation processes such as the UR (Li et al., 2019c). To further advance our knowledge of dust hazards at the regional-scale in China, the impacts of various forms of energy transport on the synoptic systems of DEs in China will be concurrently considered in future work. Globally, the majority of DAs are found in arid and semi-arid areas, and the most widespread and longest-lasting source regions of DAs are located in the NH, forming a dust belt starting from the west coast of northern Africa and extending through the Arabian Peninsula and central and southern Asia to eastern China (Washington et al., 2003; Ginoux et al., 2012). In this study, the contribution of DA source regions in East Asia to the DEs in North China is mainly considered, but insufficient consideration is given to other DA source regions. In further studies, more study methods, such as numerical simulations, should be applied to fully explore the role of DA transport from the NH source areas of DAs to China and to elucidate the details of the development of DEs in China. In addition, the DEs in China are also impacted by other factors that are related to the NAO, such as the ENSO (Li et al., 2021b; Yang et al., 2022). Previous research has demonstrated that central Pacific El Niño events can stimulate the negative phase of the NAO by transmitting the Pacific signal to the north Atlantic through a "subtropical bridge" mechanism,

while this association is insignificant for eastern Pacific El Niño events (Graf and Zanchettin, 2012). Zhang et al. (2015) also discovered that the north Atlantic jet stream strengthens and the NAO exhibits a positive phase during central Pacific La Niña events, whereas the north Atlantic jet stream weakens and the NAO exhibits a negative phase during eastern Pacific La Niña events. In the context of global warming, the SSTA of the tropical Pacific mainly exhibits a cold tongue mode, and the positive phase of the cold tongue mode can easily stimulate central Pacific El Niño events (Li et al., 2017). However, it is not clear how the connection between the NAO and ENSO will evolve under global warming. Therefore, it is worthwhile to continue researching the synergistic effect of the NAO and ENSO on the DEs in China. Furthermore, NAO is closely related to dust activities in many regions, except for China. For example, Moulin et al. (1997) and Ginoux et al. (2004) both indicated a strong correlation between NAO and dust activity in North Africa, using satellite data and dust transport models, respectively. Banerjee et al. (2021) and Li et al. (2022) emphasized the important role of NAO in the dust activities of South Asia and Central Asia. Hence, future studies are needed to explore the relationship between the dust activities in other regions and NAO.

Code and data availability. The MERRA-2 dust aerosol concentrations dataset can be downloaded from https://disc.gsfc.nasa.gov/datasets?project=MERRA-2 (last access: 12 January 2023). The atmospheric reanalysis datasets, including the wind field, geopotential height field, sea level pressure field, temperature field, and vertical velocity field can be downloaded from https://cds.climate.copernicus.eu/#!/search?text=ERA5&type=dataset (last access: 12 January 2023). Our results can be made available upon request.

Author contributions. YL, FLX, and JF conceptualized and designed the research. FLX synthesized and analysed the dataset. YL, FLX, and JF produced the figures. CL and WJZ contributed to the MERRA-2 dataset retrieval. All the authors including MYD, WJS discussed the results and wrote the paper.

Competing interests. The authors declare that they have no conflict of interest.

Acknowledgements. This research has been supported by the National Key Research & Development (R&D) Program of China (2019YFA0606800) and the National Natural Science Foundation of China (42222501 and 41975079).

Financial support. This research has been supported by the National Key Research & Development (R&D) Program of China (2019YFA0606800) and the National Natural Science Foundation of China (42222501 and 41975079).

References

Ackerman, A. S., Toon, O. B., Stevens, D. E., Heymsfield, A. J., Ramanathan, V., and Welton, E. J.: Reduction of tropical cloudiness by soot, Science, 288, 1042-1047, https://doi.org/10.1126/science.288.5468.1042, 2000.

An, L. C., Che, H. Z., Xue, M., Zhang, T. H., Wang, H., Wang, Y. Q., Zhou, C. H., Zhao, H. J., Gui, K., Zheng, Y., Sun, T. Z., Liang, Y. X., Sun, E. W., Zhang, H. D., and Zhang, X. Y.: Temporal and spatial variations in sand and dust storm events in East Asia from 2007 to 2016: Relationships with surface conditions and climate change, Sci. Total Environ., 633, 452-462, https://doi.org/10.1016/j.scitotenv.2018.03.068, 2018.

Banerjee, P., Satheesh, S. K., and Moorthy, K. K.: Is the Atlantic Ocean driving the recent variability in South Asian dust?, Atmospheric Chemistry and Physics, 21, 17665-17685, https://doi.org/10.5194/acp-21-17665-2021, 2021.

Cayan, D. R.: Latent and Sensible Heat Flux Anomalies over the Northern Oceans: The Connection to Monthly Atmospheric Circulation, J. Clim., 5, 354-369, https://doi.org/10.1175/1520-0442(1992)005<0354:Lashfa>2.0.Co;2, 1992.

Che, H. Z., Gui, K., Xia, X. G., Wang, Y. Q., Holben, B. N., Goloub, P., Cuevas-Agullo, E., Wang, H., Zheng, Y., Zhao, H. J., and Zhang, X. Y.: Large contribution of meteorological factors to inter-decadal changes in regional aerosol optical depth, Atmos. Chem. Phys., 19, 10497-10523, https://doi.org/10.5194/acp-19-10497-2019, 2019.

Chen, S. Y., Huang, J. P., Kang, L. T., Wang, H., Ma, X. J., He, Y. L., Yuan, T. G., Yang, B., Huang, Z. W., and Zhang, G. L.: Emission, transport, and radiative effects of mineral dust from the Taklimakan and Gobi deserts: comparison of measurements and model results, Atmos. Chem. Phys., 17, 2401-2421, https://doi.org/10.5194/acp-17-2401-2017, 2017.

Chiapello, I., Moulin, C., and Prospero, J. M.: Understanding the long-term variability of African dust transport across the Atlantic as recorded in both Barbados surface concentrations and large-scale Total Ozone Mapping Spectrometer (TOMS) optical thickness, J. Geophys. Res.-Atmos., 110, 9, https://doi.org/10.1029/2004jd005132, 2005.

Czaja, A. and Frankignoul, C.: Observed Impact of Atlantic SST Anomalies on the North Atlantic Oscillation, J. Clim., 15, 606-623, https://doi.org/10.1175/1520-0442(2002)015<0606:Oioasa>2.0.Co;2, 2002.

Duce, R. A., Unni, C. K., Ray, B. J., Prospero, J. M., and Merrill, J. T.: Long-Range Atmospheric Transport of Soil Dust from Asia to the Tropical North Pacific: Temporal Variability, Science, 209, 1522-1524, https://doi.org/10.1126/science.209.4464.1522, 1980.

Feng, J., Li, J. P., Liao, H., and Zhu, J. L.: Simulated coordinated impacts of the previous autumn North Atlantic Oscillation (NAO) and winter El Nino on winter aerosol concentrations over eastern China, Atmos. Chem. Phys., 19, 10787-10800, https://doi.org/10.5194/acp-19-10787-2019, 2019.

Feng, J., Zhu, J. L., Li, J. P., and Liao, H.: Aerosol concentrations variability over China: two distinct leading modes, Atmos. Chem. Phys., 20, 9883-9893, https://doi.org/10.5194/acp-20-9883-2020, 2020.

Gary, L.: Midlatitude Synoptic Meteorology Dynamics, Analysis, and Forecasting, American Meteorological Society, American, 2012.

Gelaro, R., McCarty, W., Suarez, M. J., Todling, R., Molod, A., Takacs, L., Randles, C. A., Darmenov, A., Bosilovich, M. G., Reichle, R., Wargan, K., Coy, L., Cullather, R., Draper, C., Akella, S., Buchard, V., Conaty, A., da Silva, A. M., Gu, W., Kim, G. K., Koster, R., Lucchesi, R., Merkova, D., Nielsen, J. E., Partyka, G., Pawson, S., Putman, W., Rienecker, M., Schubert, S. D., Sienkiewicz, M., and Zhao, B.: The Modern-Era Retrospective Analysis for Research and Applications, Version 2 (MERRA-2), J. Clim., 30, 5419-5454, https://doi.org/10.1175/jcli-d-16-0758.1, 2017.

Giannini, A., Kushnir, Y., and Cane, M. A.: Interannual variability of Caribbean rainfall, ENSO, and the Atlantic Ocean, J. Clim., 13, 297-311, https://doi.org/10.1175/1520-0442(2000)013<0297:Ivocre>2.0.Co;2, 2000.

Ginoux, P., Prospero, J. M., Torres, O., and Chin, M.: Long-term simulation of global dust distribution with the GOCART model: correlation with North Atlantic Oscillation, Environ. Modell. Softw., 19, 113-128, https://doi.org/10.1016/s1364-8152(03)00114-2, 2004.

Ginoux, P., Prospero, J. M., Gill, T. E., Hsu, N. C., and Zhao, M.: Global-scale attribution of anthropogenic and natural dust sources and their emission rates based on MODIS Deep Blue aerosol products, Rev. Geophys., 50, 36, https://doi.org/10.1029/2012rg000388, 2012.

Graf, H.-F. and Zanchettin, D.: Central Pacific El Niño, the "subtropical bridge," and Eurasian climate, J. Geophys. Res.-Atmos., 117, https://doi.org/10.1029/2011JD016493, 2012.

Han, Y., Wang, T. H., Tang, J. Y., Wang, C. Y., Jian, B. D., Huang, Z. W., and Huang, J. P.: New insights into the Asian dust cycle derived from CALIPSO lidar measurements, Remote Sens. Environ., 272, 15, https://doi.org/10.1016/j.rse.2022.112906, 2022.

Hartley, S. and Keables, M. J.: Synoptic associations of winter climate and snowfall variability in New England, USA, 1950-1992, Int. J. Climatol., 18, 281-298, https://doi.org/10.1002/(sici)1097-0088(19980315)18:3<281::Aid-joc245>3.0.Co;2-f, 1998.

Hersbach, H., Bell, B., Berrisford, P., Hirahara, S., Horanyi, A., Munoz-Sabater, J., Nicolas, J., Peubey, C., Radu, R., Schepers, D., Simmons, A., Soci, C., Abdalla, S., Abellan, X., Balsamo, G., Bechtold, P., Biavati, G., Bidlot, J., Bonavita, M., De Chiara, G., Dahlgren, P., Dee, D., Diamantakis, M., Dragani, R., Flemming, J., Forbes, R., Fuentes, M., Geer, A., Haimberger, L., Healy, S., Hogan, R. J., Holm, E., Janiskova, M., Keeley, S., Laloyaux, P., Lopez, P., Lupu,

C., Radnoti, G., de Rosnay, P., Rozum, I., Vamborg, F., Villaume, S., and Thepaut, J. N.: The ERA5 global reanalysis, Q. J. R. Meteorol. Soc., 146, 1999-2049, https://doi.org/10.1002/qj.3803, 2020.

Holopainen, E. O. and Oort, A. H.: On the Role of Large-Scale Transient Eddies in the Maintenance of the Vorticity and Enstrophy of the Time-Mean Atmospheric Flow, J. Atmos. Sci., 38, 270-280, https://doi.org/10.1175/1520-0469(1981)038<0270:Otrols>2.0.Co;2, 1981.

Holopainen, E. O., Rontu, L., and Lau, N. C.: The Effect of Large-Scale Transient Eddies on the Time-Mean Flow in the Atmosphere, J. Atmos. Sci., 39, 1972-1984, https://doi.org/10.1175/1520-0469(1982)039<1972:Teolst>2.0.Co;2, 1982.

Hong, S. K., Ryoo, S. B., Kim, J., and Lee, S. S.: Prediction of Asian Dust Days over Northern China Using the KMA-ADAM2 Model, Weather Forecast., 34, 1777-1787, https://doi.org/10.1175/waf-d-19-0008.1, 2019.

Huang, B. Y., Thorne, P. W., Banzon, V. F., Boyer, T., Chepurin, G., Lawrimore, J. H., Menne, M. J., Smith, T. M., Vose, R. S., and Zhang, H. M.: Extended Reconstructed Sea Surface Temperature, Version 5 (ERSSTv5): Upgrades, Validations, and Intercomparisons, J. Clim., 30, 8179-8205, https://doi.org/10.1175/jcli-d-16-0836.1, 2017.

Huang, J. P., Lin, B., Minnis, P., Wang, T. H., Wang, X., Hu, Y. X., Yi, Y. H., and Ayers, J. K.: Satellite-based assessment of possible dust aerosols semi-direct effect on cloud water path over East Asia, Geophys. Res. Lett., 33, 5, https://doi.org/10.1029/2006gl026561, 2006.

Huang, J. P., Liu, J. J., Chen, B., and Nasiri, S. L.: Detection of anthropogenic dust using CALIPSO lidar measurements, Atmos. Chem. Phys., 15, 11653-11665, https://doi.org/10.5194/acp-15-11653-2015, 2015.

Huang, J. P., Wang, T. H., Wang, W. C., Li, Z. Q., and Yan, H. R.: Climate effects of dust aerosols over East Asian arid and semiarid regions, J. Geophys. Res.-Atmos., 119, 11398-11416, https://doi.org/10.1002/2014jd021796, 2014a.

Huang, X., Song, Y., Zhao, C., Li, M. M., Zhu, T., Zhang, Q., and Zhang, X. Y.: Pathways of sulfate enhancement by natural and anthropogenic mineral aerosols in China, J. Geophys. Res.-Atmos., 119, 14165-14179, https://doi.org/10.1002/2014jd022301, 2014b.

Huang, Y. H., Liu, X. D., Yin, Z. Y., and An, Z. S.: Global Impact of ENSO on Dust Activities with Emphasis on the Key Region from the Arabian Peninsula to Central Asia, J. Geophys. Res.-Atmos., 126, 24, https://doi.org/10.1029/2020jd034068, 2021.

Hurrell, J. W.: Decadal Trends in the North Atlantic Oscillation: Regional Temperatures and Precipitation, Science, 269, 676-679, https://doi.org/10.1126/science.269.5224.676, 1995.

Ji, L. Q. and Fan, K.: Climate prediction of dust weather frequency over northern China based on sea-ice cover and vegetation variability, Clim. Dyn., 53, 687-705, https://doi.org/10.1007/s00382-018-04608-w, 2019.

Jin, F. F., Pan, L. L., and Watanabe, M.: Dynamics of synoptic eddy and low-frequency flow interaction. Part I: A linear closure, J. Atmos. Sci., 63, 1677-1694, https://doi.org/10.1175/jas3715.1, 2006.

Kang, L. T., Huang, J. P., Chen, S. Y., and Wang, X.: Long-term trends of dust events over Tibetan Plateau during 1961-2010, Atmos. Environ., 125, 188-198, https://doi.org/10.1016/j.atmosenv.2015.10.085, 2016.

Kaufman, Y. J., Tanre, D., and Boucher, O.: A satellite view of aerosols in the climate system, Nature, 419, 215-223, https://doi.org/10.1038/nature01091, 2002.

Kurosaki, Y. and Mikami, M.: Recent frequent dust events and their relation to surface wind in East Asia, Geophys. Res. Lett., 30, 4, https://doi.org/10.1029/2003gl017261, 2003.

Kutiel, H. and Furman, H.: Dust storms in the Middle East: Sources of origin and their temporal characteristics, Indoor Built Environ., 12, 419-426, https://doi.org/10.1177/1420326x03037110, 2003.

Lau, N. C. and Nath, M. J.: Variability of the Baroclinic and Barotropic Transient Eddy Forcing Associated with Monthly Changes in the Midlatitude Storm Tracks, J. Atmos. Sci., 48, 2589-2613, https://doi.org/10.1175/1520-0469(1991)048<2589:Votbab>2.0.Co;2, 1991.

Lee, E. H. and Sohn, B. J.: Examining the impact of wind and surface vegetation on the Asian dust occurrence over three classified source regions, J. Geophys. Res.-Atmos., 114, 12, https://doi.org/10.1029/2008jd010687, 2009.

Li, J., Garshick, E., Huang, S. D., and Koutrakis, P.: Impacts of El Nino-Southern Oscillation on surface dust levels across the world during 1982-2019, Sci. Total Environ., 769, 7, https://doi.org/10.1016/j.scitotenv.2020.144566, 2021b.

Li, J. P. and Wang, J. X. L.: A new North Atlantic Oscillation index and its variability, Adv. Atmos. Sci., 20, 661-676, https:// doi.org/10.1007/BF02915394, 2003.

Li, J. P., Zheng, F., Sun, C., Feng, J., and Wang, J.: Pathways of Influence of the Northern Hemisphere Mid-high Latitudes on East Asian Climate: A Review, Adv. Atmos. Sci., 36, 902-921, https://doi.org/10.1007/s00376-019-8236-5, 2019a.

Li, M. Y., Yao, Y., Simmonds, I., Luo, D. H., Zhong, L. H., and Pei, L.: Linkages between the atmospheric transmission originating from the North Atlantic Oscillation and persistent winter haze over Beijing, Atmos. Chem. Phys., 21, 18573-18588, https://doi.org/10.5194/acp-21-18573-2021, 2021a.

Li, X., Liu, X. D.: Relation of Spring Dust-Storm Activities in Northern China and Changes of Upper Westerlies, Plateau. Meteorology (in Chinese)., 34, 1292-1300, https://doi.org/10.7522/j.issn.1000-0534.2014.00067, 2015.

Li, Y., Hu, X. L., Wang, X., and Ji, M. X.: Impact of transient eddy fluxes on the dust storm event: Cases study in South Xinjiang, China, Atmos. Res., 269, 11, https://doi.org/10.1016/j.atmosres.2022.106054, 2022.

Li, Y., Li, J. P., Zhang, W. J., Chen, Q. L., Feng, J., Zheng, F., Wang, W., and Zhou, X.: Impacts of the Tropical Pacific Cold Tongue Mode on ENSO Diversity Under Global Warming, J. Geophys. Res.-Oceans, 122, 8524-8542, https://doi.org/10.1002/2017jc013052, 2017.

Li, Y., Lu, Y., and Wang, C. H.: Characteristics of thermal and momentum transport during the lifetime of Ural blocking highs, Int. J. Climatol., 40, 77-93, https://doi.org/10.1002/joc.6195, 2019c.

Li, Y., Song, Y. G., Kaskaoutis, D. G., Zhang, X. X., Chen, X. L., Shukurov, N., and Orozbaev, R.: Atmospheric dust dynamics over Central Asia: A perspective view from loess deposits, Gondwana Res., 109, 150-165, https://doi.org/10.1016/j.gr.2022.04.019, 2022.

Li, Y., Zhang, J. Y., Lu, Y., Zhu, J. L., and Feng, J.: Characteristics of Transient Eddy Fluxes during Blocking Highs Associated with Two Cold Events in China, Atmosphere, 10, 15, https://doi.org/10.3390/atmos10050235, 2019b.

Lin, H. and Wu, Z. W.: Contribution of the Autumn Tibetan Plateau Snow Cover to Seasonal Prediction of North American Winter Temperature, J. Clim., 24, 2801-2813, https://doi.org/10.1175/2010jcli3889.1, 2011.

Liu, J., Wu, D. Y., Liu, G. J., Mao, R., Chen, S. Y., Ji, M. X., Fu, P. Q., Sun, Y. L., Pan, X. L., Jin, H. C., Zhou, Y. B., and Wang, X.: Impact of Arctic amplification on declining spring dust events in East Asia, Clim. Dyn., 54, 1913-1935, https://doi.org/10.1007/s00382-019-05094-4, 2020.

Liu, X. D. and Yin, Z. Y.: Spatial and temporal variation of summer precipitation over the eastern Tibetan Plateau and the North Atlantic oscillation, J. Clim., 14, 2896-2909, https://doi.org/10.1175/1520-0442(2001)014<2896:Satvos>2.0.Co;2, 2001.

Liu, X. D., Yin, Z. Y., Zhang, X. Y., and Yang, X. C.: Analyses of the spring dust storm frequency of northern China in relation to antecedent and concurrent wind, precipitation, vegetation, and soil moisture conditions, J. Geophys. Res.-Atmos., 109, 16, https://doi.org/10.1029/2004jd004615, 2004.

Liu, Y. Q., Zhang, J. H., Zhou, P. T., Lin, T., Hong, J., Shi, L. M., Yao, F. M., Wu, J., Guo, H. D., and Leeuw, G.: Satellite-based estimate of the variability of warm cloud properties associated with aerosol and meteorological conditions, Atmospheric Chemistry and Physics, 18, 18187-18202, https://doi.org/10.5194/acp-18-18187-2018, 2018.

Mao, R., Ho, C. H., Shao, Y., Gong, D. Y., and Kim, J.: Influence of Arctic Oscillation on dust activity over northeast Asia, Atmos. Environ., 45, 326-337, https://doi.org/10.1016/j.atmosenv.2010.10.020, 2011.

Moulin, C., Lambert, C. E., Dulac, F., and Dayan, U.: Control of atmospheric export of dust from North Africa by the North Atlantic oscillation, Nature, 387, 691-694, https://doi.org/10.1038/42679, 1997.

Nie, W., Ding, A. J., Wang, T., Kerminen, V. M., George, C., Xue, L. K., Wang, W. X., Zhang, Q. Z., Petaja, T., Qi, X. M., Gao, X. M., Wang, X. F., Yang, X. Q., Fu, C. B., and Kulmala, M.: Polluted dust promotes new particle formation and growth, Sci Rep, 4, 6634, https://doi.org/10.1038/srep08949, 2015.

Qian, W. H.: Physical decomposition principle of regional-scale atmospheric transient anomaly, J. Geophys (in Chinese)., 55, 1439-1448, https://doi.org/10.6038/j.issn.0001-5733.2012.05.002, 2012.

Sassen, K., DeMott, P. J., Prospero, J. M., and Poellot, M. R.: Saharan dust storms and indirect aerosol effects on clouds: CRYSTAL-FACE results, Geophys. Res. Lett., 30, https://doi.org/10.1029/2003GL017371, 2003.

Shao, T. H., Zhang, Y. C.: Influence of Winter North Atlantic Oscillation on Spring Precipitation in China, Plateau. Meteorology (in Chinese)., 31, 1225-1233, https://doi.org/CNKI:SUN:GYQX.0.2012-05-006, 2012.

Sokolik, I. N. and Toon, O. B.: Direct radiative forcing by anthropogenic airborne mineral aerosols, Nature, 381, 681-683, https://doi.org/10.1038/381681a0, 1996.

Solomon, A. B.: An observational study of the spatial and temporal scales of transient eddy sensible heat fluxes, J. Clim., 10, 508-520, https://doi.org/10.1175/1520-0442(1997)010<0508:Aosots>2.0.Co;2, 1997.

Tang, H. Y., Zhai, P. M., and Chang, Y. K.: SVD Analysis between Northern Hemisphere 500 hPa Heights and Spring Duststorms over Northern China, J. Dersert. Res (in Chinese)., 25, 570-576, https://doi.org/10.3321/j.issn:1000-694X.2005.04.020, 2005.

Trenberth, K. E.: An assessment of the impact of transient eddies on the zonal flow during a blocking episode using localized Eliassen-Palm flux diagnostics, J. Atmos. Sci., 43, 2070-2087,

https://doi.org/10.1175/1520-0469(1986)043<2070:Aaotio>2.0.Co;2, 1986.

Walker, G. T.: Correlations in seasonal variations of weather IX, Indian Meteor. Dept., 24, 275–332, 1924.

Wang, X., Liu, J., Che, H. Z., Ji, F., and Liu, J. J.: Spatial and temporal evolution of natural and anthropogenic dust events over northern China, Sci Rep, 8, 2141, https://doi.org/10.1038/s41598-018-20382-5, 2018.

Wang, X. M., Zhai, P. M., and Wang, C. C.: Variations in extratropical cyclone activity in northern East Asia, Adv. Atmos. Sci., 26, 471-479, https://doi.org/10.1007/s00376-009-0471-8, 2009.

Wang, Y. B., Shi, N.: Relation of North Atlantic Oscillation Anomaly to China Climate during 1951-1995, Trans. Atmos. Sci (in Chinese)., 24, 315-322, https://doi.org/10.3969/j.issn.1674-7097.2001.03.003, 2001.

Wang, Z. Q., Yang, S., Lau, N. C., and Duan, A. M.: Teleconnection between Summer NAO and East China Rainfall Variations: A Bridge Effect of the Tibetan Plateau, J. Clim., 31, 6433-6444, https://doi.org/10.1175/jcli-d-17-0413.1, 2018.

Washington, R., Todd, M., Middleton, N. J., and Goudie, A. S.: Dust-storm source areas determined by the total ozone monitoring spectrometer and surface observations, Ann. Assoc. Am. Geogr., 93, 297-313, https://doi.org/10.1111/1467-8306.9302003, 2003.

Watanabe, M.: Asian jet waveguide and a downstream extension of the North Atlantic Oscillation, J. Clim., 17, 4674-4691, https://doi.org/10.1175/jcli-3228.1, 2004.

Watanabe, M. and Kimoto, M.: Atmosphere-ocean thermal coupling in the North Atlantic: A positive feedback, Q. J. R. Meteorol. Soc., 126, 3343–3369, https://doi.org/10.1002/qj.49712657017, 2000.

Wilcox, L. J., Liu, Z., Samset, B. H., Hawkins, E., Lund, M. T., Nordling, K., Undorf, S., Bollasina, M., Ekman, A. M. L., Krishnan, S., Merikanto, J., and Turner, A. G.: Accelerated increases in global and Asian summer monsoon precipitation from future aerosol reductions, Atmospheric Chemistry and Physics, 20, 11955-11977, https://doi.org/10.5194/acp-20-11955-2020, 2020.

Wu, J., Kurosaki, Y., Shinoda, M., and Kai, K. J.: Regional Characteristics of Recent Dust Occurrence and Its Controlling Factors in East Asia, Sola, 12, 187-191, https://doi.org/10.2151/sola.2016-038, 2016.

Wu, Z. W., Wang, B., Li, J. P., and Jin, F. F.: An empirical seasonal prediction model of the east Asian summer monsoon using ENSO and NAO, J. Geophys. Res.-Atmos., 114, 13, https://doi.org/10.1029/2009jd011733, 2009.

Yang, Y., Russell, L. M., Lou, S. J., Liao, H., Guo, J. P., Liu, Y., Singh, B., and Ghan, S. J.: Dust-wind interactions can intensify aerosol pollution over eastern China, Nat. Commun., 8, 8, https://doi.org/10.1038/ncomms15333, 2017.

Yang, Y., Zeng, L., Wang, H., Wang, P., and Liao, H.: Dust pollution in China affected by different spatial and temporal types of El Niño, Atmos. Chem. Phys., 22, 14489-14502, https://doi.org/10.5194/acp-22-14489-2022, 2022.

Yao, W. R., Gui, K., Wang, Y. Q., Che, H. Z., and Zhang, X. Y.: Identifying the dominant local factors of 2000-2019 changes in dust loading over East Asia, Sci. Total Environ., 777, 10, https://doi.org/10.1016/j.scitotenv.2021.146064, 2021.

Yao, Y., Zhang, W. Q., Luo, D. H., Zhong, L. H., and Pei, L.: Seasonal Cumulative Effect of Ural Blocking Episodes on the Frequent Cold events in China during the Early Winter of 2020/21, Adv. Atmos. Sci., 39, 609-624, https://doi.org/10.1007/s00376-021-1100-4, 2022.

Yin, Z. C., Wan, Y., Zhang, Y. J., and Wang, H. J.: Why super sandstorm 2021 in North China?, Natl. Sci. Rev., 9, 9, https://doi.org/10.1093/nsr/nwab165, 2021.

Yu, B., Lin, H., Wu, Z. W., and Merryfield, W. J.: Relationship between North American winter temperature and large-scale atmospheric circulation anomalies and its decadal variation, Environ. Res. Lett., 11, 8, https://doi.org/10.1088/1748-9326/11/7/074001, 2016.

Yu, X. C., Wang, Z. L., Zhang, H., and Zhao, S. Y.: Impacts of different types and intensities of El Niño events on winter aerosols over China, Sci. Total Environ., 655, 766-780, https://doi.org/10.1016/j.scitotenv.2018.11.090, 2019.

Zender, C. S., Miller, R. L., and Tegen, I.: Quantifying mineral dust mass budgets:Terminology, constraints, and current estimates, Eos, Transactions American Geophysical Union, 85, 509-512, https://doi.org/10.1029/2004EO480002, 2004.

Zhang, C. X., Liu, C., Hu, Q. H., Cai, Z. N., Su, W. J., Xia, C. Z., Zhu, Y. Z., Wang, S. W., and Liu, J. G.: Satellite UV-Vis spectroscopy: implications for air quality trends and their driving forces in China during 2005-2017, Light-Sci. Appl., 8, 12, https://doi.org/10.1038/s41377-019-0210-6, 2019.

Zhang, L., Zhang, H. S., Li, Q. H., Cai, X. H., and Song, Y.: Vertical dispersion mechanism of long-range transported dust in Beijing: Effects of atmospheric turbulence, Atmos. Res., 269, 12, https://doi.org/10.1016/j.atmosres.2022.106033, 2022.

Zhang, P., Wu, Z. W., and Jin, R.: How can the winter North Atlantic Oscillation influence the early summer precipitation in Northeast Asia: effect of the Arctic sea ice, Clim. Dyn., 56, 1989-2005, https://doi.org/10.1007/s00382-020-05570-2, 2021.

Zhang, W. J., Wang, L., Xiang, B. Q., Qi, L., and He, J. H.: Impacts of two types of La Nina on the NAO during boreal winter, Clim. Dyn., 44, 1351-1366, https://doi.org/10.1007/s00382-014-2155-z, 2015.

Zhang, X. Y., Gong, S. L., Zhao, T. L., Arimoto, R., Wang, Y. Q., and Zhou, Z. J.: Sources of Asian dust and role of climate change versus desertification in Asian dust emission, Geophys. Res. Lett., 30, 4, https://doi.org/10.1029/2003gl018206, 2003.

Zhang, X. Y., Wang, Y. Q., Niu, T., Zhang, X. C., Gong, S. L., Zhang, Y. M., and Sun, J. Y.: Atmospheric aerosol compositions in China: spatial/temporal variability, chemical signature, regional haze distribution and comparisons with global aerosols, Atmos. Chem. Phys., 12, 6273-6273, https://doi.org/10.5194/acp-12-6273-2012, 2012.

Zhao, S., Li, J. P., and Sun, C.: Decadal variability in the occurrence of wintertime haze in central eastern China tied to the Pacific Decadal Oscillation, Sci Rep, 6, 9, https://doi.org/10.1038/srep27424, 2016.

Zhao, Y., Li, H. J., and He, Q.: Variation of dust strom days in Tarim Basin and its relation with North Atlantic Oscillation, J. Dersert. Res (in Chinese)., 32, 1082-1088, https://doi.org/CNKI:SUN:ZGSS.0.2012-04-027, 2012.

Zuo, J. Q., Ren, H. L., and Li, W. J.: Contrasting Impacts of the Arctic Oscillation on Surface Air Temperature Anomalies in Southern China between Early and Middle-to-Late Winter, J. Clim., 28, 4015-4026, https://doi.org/10.1175/jcli-d-14-00687.1, 2015.